

## Distribution Network Reconfiguration Considering the Impacts of Local Renewable Generation and External Power Grid

Li, Haixiao; Lekic, Aleksandra; Li, Shan; Jiang, Dongrong; Guo, Qiang; Zhou, Lin

**DOI**

[10.1109/TIA.2023.3307070](https://doi.org/10.1109/TIA.2023.3307070)

**Publication date**

2023

**Document Version**

Final published version

**Published in**

IEEE Transactions on Industry Applications

**Citation (APA)**

Li, H., Lekic, A., Li, S., Jiang, D., Guo, Q., & Zhou, L. (2023). Distribution Network Reconfiguration Considering the Impacts of Local Renewable Generation and External Power Grid. *IEEE Transactions on Industry Applications*, 59(6), 7771-7788. <https://doi.org/10.1109/TIA.2023.3307070>

**Important note**

To cite this publication, please use the final published version (if applicable).  
Please check the document version above.

**Copyright**

Other than for strictly personal use, it is not permitted to download, forward or distribute the text or part of it, without the consent of the author(s) and/or copyright holder(s), unless the work is under an open content license such as Creative Commons.

**Takedown policy**

Please contact us and provide details if you believe this document breaches copyrights.  
We will remove access to the work immediately and investigate your claim.

***Green Open Access added to TU Delft Institutional Repository***

***'You share, we take care!' - Taverne project***

**<https://www.openaccess.nl/en/you-share-we-take-care>**

Otherwise as indicated in the copyright section: the publisher is the copyright holder of this work and the author uses the Dutch legislation to make this work public.

# Distribution Network Reconfiguration Considering the Impacts of Local Renewable Generation and External Power Grid

Haixiao Li <sup>1b</sup>, Aleksandra Lekić <sup>1b</sup>, Senior Member, IEEE, Shan Li <sup>1b</sup>, Dongrong Jiang <sup>1b</sup>, Qiang Guo <sup>1b</sup>, and Lin Zhou <sup>1b</sup>

**Abstract**—The distribution network (DN) reconfiguration is a well-known optimal power flow (OPF) problem. However, with the transition of DN from “passive” to “active”, new technical challenges arise in DN reconfiguration. This article addresses two key issues in this regard. Firstly, the integration of local renewable generation (LRG) introduces uncertainty into the system-wide power flow of the DN. Secondly, the coupling between DN and the external power grid (EPG) affects the determination of DN root voltage. Consequently, a novel DN reconfiguration approach is proposed in this article. To begin with, an explicit mixed-integer convex OPF model is constructed that incorporates both the EPG and DN sides. Notably, the OPF model embeds the function of local droop control that is provided by LRG. Subsequently, the original OPF model is decomposed, and the distributed optimization methods based on the augmented Lagrangian relaxation are employed. The article comprehensively discusses parallel processing and asynchronous implementation as parts of the distributed optimization procedure. Furthermore, to address the uncertainty related to LRG integration, the extreme scenario method is used to provide a robust decision regarding DN reconfiguration. The application of the extreme scenario method in the distributed OPF model concerning DN reconfiguration is successively developed. Finally, numerical results are presented to demonstrate the acceptable performance of the distributed optimization methods, in terms of optimality and convergence. Also, these are validated that the proposed DN reconfiguration approach exhibits robustness to LRG integration,

the system-wide voltage profile is improved, and the active power loss is effectively reduced using the proposed DN reconfiguration approach.

**Index Terms**—Augmented Lagrangian relaxation, distribution network reconfiguration, external power grid (EPG), extreme scenario method, local renewable energy (LRG).

## NOMENCLATURE

### Abbreviation

ATC	Analytical target cascading.
ADMM	Alternating direction method of multipliers.
APP	Auxiliary problem principle.
DN	Distribution network.
EPG	External power grid.
LRG	Local renewable generation.
LDC	Local droop control.
OLTC	On-load tap changer.
SOC	Second-order conic.

### Indices and Sets

$i, j$	Indices for nodes.
$ij, hi$	Indices for branches.
$\mathcal{N}_{EPG}, \mathcal{N}_{DN}$	Sets of nodes on EPG and DN sides.
$\mathcal{F}_i, \mathcal{D}_i$	Sets of father node and descendant node for node $i$ .
$\ell_{EPG}, \ell_{DN}$	Set of branches on EPG and DN sides.
$\mathcal{S}, \mathcal{E}$	Sets that cover all the uncertain and Extreme scenarios related to LRG integration.
$\mathcal{G}, \mathcal{H}$	The general form of equality and quality constraints.

### Parameters and Functions

$g_{ij}, b_{ij}$	Conductivity and susceptance for a branch $ij$ .
$r_{ij}, x_{ij}$	Resistance and inductance for a branch $ij$ .
$s_{i,G}^{\text{rated}}, s_{i,LRG}^{\text{rated}}$	Rated capacities for the generating system and LRG at node $i$ .
$u_i^{\min}, u_i^{\max}$	Minimum and maximum values for the voltage security bound at node $i$ .
$u_{i,DB}^{\min}, u_{i,DB}^{\max}$	Minimum and maximum values for the dead-zone bound of LDC at node $i$ .

Manuscript received 15 December 2022; revised 7 June 2023; accepted 23 July 2023. Date of publication 22 August 2023; date of current version 22 November 2023. Paper 2022-IACC-1477.R1, presented at the 2021 IEEE 2nd China International Youth Conference on Electrical Engineering, Chengdu, China, Dec. 15–17, and approved for publication in the IEEE TRANSACTIONS ON INDUSTRY APPLICATIONS by the Industrial Automation and Control Committee of the IEEE Industry Applications Society [DOI: 10.1109/CIYCEE53554.2021.9676732]. This work was supported in part by Natural Science Foundation of Chongqing under Grant CSTB2022NSCQ-MSX0997, in part by the Science and Technology Research Program of Chongqing Municipal Education Commission under Grant KJQN202201153, and in part by the Scientific Research Starting Foundation of Chongqing University of Technology under Grant 2021ZDZ013. (Corresponding author: Qiang Guo.)

Haixiao Li, Shan Li, Dongrong Jiang, and Qiang Guo are with Chongqing Energy Internet Engineering Technology Research Center, Chongqing University of Technology, Chongqing 400054, China (e-mail: 394190414@qq.com; lishan@cqut.edu.cn; drjiang@126.com; guoqiang@cqut.edu.cn).

Aleksandra Lekić is with the Department of Electrical Sustainable Energy, Delft University of Technology, 2628 Delft, The Netherlands (e-mail: a.lekic@tudelft.nl).

Lin Zhou is with the State Key Laboratory of Power Transmission Equipment & System Security and New Technology, Chongqing University, Chongqing 400044, China (e-mail: zhoulin@cqu.edu.cn).

Color versions of one or more figures in this article are available at <https://doi.org/10.1109/TIA.2023.3307070>.

Digital Object Identifier 10.1109/TIA.2023.3307070

$p_{i,LRG}^{MPPT}$	Maximum power point tracking value of active power output for LRG at node $i$ .
$\kappa_i^{left}, \kappa_i^{right}$	Droop slopes in the left and right droop zones of LDC at node $i$ .
$\varphi_i^{cap}, \varphi_i^{ind}$	Limits for capacitive and inductive power factors for generating system at node $i$ .
$\varepsilon_p, \varepsilon_d$	Primary and dual residuals for the augmented Lagrangian relaxation-based distributed optimization methods.
M	A Large positive constant for big-M relaxation.
D	Dimension of the coupled boundary variables between DN and EPG.
$C_{i,G}(\cdot)$	Generation cost function at node $i$
$Nums(\cdot)$	Symbol function to count the number of uncertain and extreme scenarios.
<i>Continuous Variables</i>	
$p_i, q_i$	Active and reactive power injection at node $i$ .
$p_{ij}, q_{ij}$	Active and reactive power flowing on branch $ij$ .
$p_{i,G}, q_{i,G}$	Active and reactive power outputs of generating station at node $i$ .
$p_{i,LRG}, q_{i,LRG}$	Active and reactive power outputs of LRG at node $i$ .
$p_{i,L}, q_{i,L}$	Active and reactive power consumption of load at node $i$ .
$v_i, u_i$	Voltage amplitude and the squared voltage amplitude at node $i$ .
$e_i, f_i$	Real and imaginary parts for the voltage at node $i$ .
$\theta_{ij}$	Difference of voltage phase between nodes $i$ and $j$ .
$q_{i,LRG}^{sat,min}, q_{i,LRG}^{sat,max}$	Minimum and maximum values of the saturation bound for LDC at node $i$ .
$q_{i,LRG}^{def}$	Default reactive power output for LDC at node $i$ .
$u_B, p_B, q_B$	Boundary variables between EPG and DN regarding the squared voltage amplitude, active power injection, and reactive power injection.
<i>Integer and Binary Variables</i>	
$\alpha_{ij}$	Link status of branches.
$K_T$	The ratio of OLTC.

## I. INTRODUCTION

**R**ECONFIGURATION of the distribution network (DN) has been a research interest as crucial for DN restoration. Back in 1988, the groundbreaking work was laid in [1]. Following that, some preliminary studies based on the heuristic approach were conducted in [2], [3], [4]. These studies were limited to the small-scale DN since DN reconfiguration is a challenging optimal power flow (OPF) problem. Generally, DN reconfiguration is modeled as a mixed-integer nonlinear OPF problem, where integer variables are usually associated with

the link status of branches and nonlinear constraints are usually associated with the power flow equations. Various works on OPF-solving approaches that have been carried out [5], [6], [7], [8], [9], [10], [11], [12], [13], [14], [15], [16], and they can be broadly classified into two paradigms: metaheuristic techniques and mathematical programming methods.

Metaheuristic techniques are mostly inspired by natural phenomena or biological processes, and they have been widely used to cope with nonconvex OPF problems in engineering practice. Metaheuristic techniques solve the optimization problems by searching in solution space using the specific rules for diversifying and intensifying initial solutions. In the 90s, the seminal study that used simulated annealing to solve the optimization problem for DN reconfiguration was published in [5]. Various metaheuristic techniques have been successfully applied to the DN reconfiguration problem. For instance, different versions of particle swarm optimization [6], [7], genetic algorithm [8], [9], tabu search [10], etc. In general, metaheuristic techniques have advantages in solving optimization problems due to their model-free characteristics and straightforward implementation that do not require explicit mathematical formulation. As a result, although DN reconfiguration formulated as a mixed-integer nonlinear OPF problem is intractable, metaheuristic techniques can be easily applied. However, metaheuristic techniques have significant drawbacks in that they are typically time-consuming and impractical for ensuring high-quality optimization solutions.

In contrast, mathematical programming methods excel at computation efficiency and can obtain high-quality optimal solutions. It would be highly desirable to convert the OPF problem involving DN reconfiguration into a specific formulation that can be directly solved using mathematical programming methods. The key step is to handle the nonlinear and nonconvex conventional power flow equations, and two approaches are commonly used: 1) linearization on power flow equations. 2) convex relaxation on power flow constraints. In [11], a mixed-integer and conic programming model based on the second-order cone (SOC) relaxation of power flow equations was proposed to minimize power loss for DN reconfiguration. [12] proposed a mixed-integer and linear programming method to determine the minimal combination of switching operations, taking linearized DistFlow [13]. In addition, spanning tree constraints to make DN radial are typically added to the optimal DN reconfiguration problem [11], [12], [14], [15], [16].

Aside from problem-solving approaches, research interest in the impacts of local renewable generation (LRG) penetration on DN reconfiguration has gradually grown in recent years. The uncertainty related to LRG integration is a prominent issue that influences system-wide power flow heavily, which will further affect the decision-making in DN reconfiguration. Two mainstream approaches to deal with this issue are: 1) stochastic optimization [17], [18], in which chance constraints are built and LRG output is analyzed as a probability distribution function. 2) robust optimization [19], [20], where LRG output is described as an uncertainty bound. Despite significant research achievements in stochastic optimization and robust optimization, there is still a need for further improvement in terms of the tractability and

scalability of the stochastic and robust optimization models. Specifically, these models cannot be solved directly using off-the-shelf solvers.

Not limited to the uncertainty associated with LRG integration, the ancillary services provided by LRG will also pose significant effects on DN reconfiguration. One of the most typical ancillary services is the local droop control (LDC) [21], [22], [23], which can quickly respond to sudden changes in the node voltage by adjusting the reactive power output of LRG. However, the importance of LDC has not been adequately recognized for DN reconfiguration. Furthermore, the aforementioned studies have all made the assumption that DN and external power grid (EPG) operate independently. In this case, the root node voltage of DN is assumed to be constant. However, as the coupling between DN and EPG is enhanced [24], [25], it is necessary to fully consider the interaction between EPG and DN, particularly the interaction impact on DN root voltage. This necessity arises from the fact that the system-wide voltage is derived from the root node voltage for DN.

According to the literature review mentioned above, it is important to give sufficient attention to the impacts of LRG and EPG on DN reconfiguration. The following aspects provide motivation for improving approaches of DN reconfiguration:

- Maintaining an optimal system-wide voltage profile is crucial for DN operation. In addition to the actions of the legacy voltage regulating devices (e.g., on-load tap changers (OLTCs)), it is essential to consider the impact of LRG equipped with LDC on the system-wide voltage adjustment.
- As the coupling between EPG and DN gets more intensive, reconfiguration for one DN becomes more closely linked to the operational status of the EPG and other DNs. The root node voltage, which serves as the coupling boundary node voltage, needs to be calculated more accurately through an integrated model that incorporates both EPG and DN, rather than being conventionally treated as a fixed swing node voltage.
- The uncertain power outputs from LRG significantly affect the accuracy of acquiring the DN power flow profile. Accordingly, the uncertainty regarding LRG should be addressed for DN reconfiguration and a tractable OPF model concerning DN reconfiguration should be developed.

In this work, we aim to realize the optimal DN reconfiguration and propose an explicit mixed-integer convex OPF model that incorporates DN and EPG sides. This article represents a substantial expansion of our previous work in [26] by broadening the literature review, considering the uncertainty associated with LRG integration and the voltage adjustment from LDC, diversifying the distributed optimization method applied in solving the proposed OPF model, and presenting a more comprehensive discussion. The following are the main contributions of our study.

- An explicit mixed-integer convex OPF model for DN reconfiguration is developed in this study. This model takes into account the coupling between the DN and EPG, enabling a more accurate calculation on the DN root voltage. Moreover, the specific piecewise function of LDC

provided by LRG is incorporated into the constructed OPF model.

- Considering data privacy and computation efforts, it is impractical to perform global optimization that incorporates both EPG and DN sides. Accordingly, the augmented Lagrangian relaxation-based distributed optimization methods are employed, such as analytical target cascading (ATC) [27], [28], alternating direction method of multipliers (ADMM) [29], [30], [31], and auxiliary problem principle (APP) [32], [33]. Furthermore, this study extensively discusses parallel processing and asynchronous implementation techniques that are relevant to the distributed optimization procedure.
- Instead of utilizing stochastic and robust optimization methods, the extreme scenario method [34], [35], [36] is employed to address the uncertainty associated with LRG integration. The extreme scenario method is chosen for its simplicity in implementation, and the resulting extreme scenario set enables covering all of the solution spaces regarding uncertain LRG outputs while avoiding the massive sampling like in the Monte Carlo method. Besides, this study extends the application of the extreme scenario method in the distributed OPF model involving DN reconfiguration.

The article begins with the mathematical formulation of the OPF model involving DN reconfiguration and embedding LDC in Section II. Then, the distributed optimization methods based on the augmented Lagrangian relaxation are illustrated in Section III. Next, the application of the extreme scenario method is introduced in Section IV. Numerical results are presented and discussed in Section V, followed by the conclusions in Section VI.

## II. OPTIMAL DN RECONFIGURATION MODEL

In this section, an optimal DN reconfiguration model that incorporates EPG and DN sides is presented.

### A. Objective Function

The joint optimization objective on EPG and DN sides is formulated as below:

$$\begin{aligned} \min \quad & \underbrace{\sum_i (p_{i,G} - p_{i,L}) + C_{i,G}}_{:=f_{\text{EPG}}}, \forall i \in \mathcal{N}_{\text{EPG}} \\ & + \underbrace{\sum_{ij} r_{ij}(p_{ij}^2 + q_{ij}^2)/v_i^2 + \sum_i (u_i - 1)^2}_{:=f_{\text{DN}}}, \forall ij \in \ell_{\text{DN}}, \forall i \in \mathcal{N}_{\text{DN}}, \end{aligned} \quad (1a)$$

$$C_{i,G}(p_{i,G}) := a_i^0 + a_i^1 p_{i,G} + a_i^2 p_{i,G}^2, \forall i \in \mathcal{N}_{\text{EPG}}, \quad (1b)$$

where  $f_{\text{EPG}}$  in (1a) considers minimizing the active power loss and the total generation cost together.  $a_i^0$ ,  $a_i^1$ , and  $a_i^2$  in (1b) are the generation cost coefficients of  $C_{i,G}$ .  $f_{\text{DN}}$  in (1a) considers minimizing the active power loss and the general voltage deviation together. Usually, the nonconvex term  $r_{ij}(p_{ij}^2 + q_{ij}^2)/(v_i^2)$

can be simplified to  $r_{ij}(p_{ij}^2 + q_{ij}^2)$  due to the assumption that  $v_i \approx 1$  p.u.,  $i \in \mathcal{N}_{\text{DN}}$ . Note that the active power loss in  $f_{\text{EPG}}$  and  $f_{\text{DN}}$  are not formulated consistently since different power flow constraints are adopted on EPG and DN sides, which will be presented in the following. “:=” used for the function and matrix definition, or variable assignment, which will frequently appear in the subsequent text.

### B. Node Power Balance Constraint

The node power balance constraint on EPG and DN sides are presented as follows:

$$\begin{cases} p_i = p_{i,G} - p_{i,L} \\ q_i = q_{i,G} - q_{i,L} \end{cases}, \forall i \in \mathcal{N}_{\text{EPG}}, \quad (2a)$$

$$\begin{cases} p_i = p_{i,\text{LRG}} - p_{i,L} \\ q_i = q_{i,\text{LRG}} - q_{i,L} \end{cases}, \forall i \in \mathcal{N}_{\text{DN}}, \quad (2b)$$

where (2a) indicates that the node power injection originates from the generating system on EPG side. Equation (2b) indicates that the node power injection originates from LRG on DN side.

### C. Power Flow Constraint

The conventional power flow constraint is shown as below:

$$p_i = v_i \sum_j v_j (g_{ij} \cos \theta_{ij} + b_{ij} \sin \theta_{ij}),$$

$$\forall i, j \in \mathcal{N}_{\text{DN}} \cup \mathcal{N}_{\text{EPG}}, \forall ij \in \ell_{\text{DN}} \cup \ell_{\text{EPG}}, \quad (3a)$$

$$q_i = v_i \sum_j v_j (g_{ij} \sin \theta_{ij} + b_{ij} \cos \theta_{ij}),$$

$$\forall i, j \in \mathcal{N}_{\text{DN}} \cup \mathcal{N}_{\text{EPG}}, \forall ij \in \ell_{\text{DN}} \cup \ell_{\text{EPG}}. \quad (3b)$$

It can be found that (3) makes OPF model hard to be solved via mathematical programming methods since they are nonconvex and nonlinear.

For EPG side, SOC relaxation on (3), as described in [37], can be used to form the convex power flow constraint. Given as  $c_{ij} := e_i e_j + f_i f_j$ ,  $s_{ij} := e_i f_j - e_j f_i$ , then  $c_{ij} = c_{ji}$ ,  $s_{ij} = -s_{ji}$ ,  $c_{ii} = v_i^2 = u_i$ , and  $c_{jj} = v_j^2 = u_j$  hold, and we have SOC relaxed power flow constraint presented as below:

$$\begin{cases} p_i = \sum_{ij} (c_{ij} g_{ij} - s_{ij} b_{ij}) \\ q_i = -\sum_{ij} (s_{ij} g_{ij} + c_{ij} b_{ij}) \\ c_{ij}^2 + s_{ij}^2 \leq c_{ii} c_{jj} \end{cases}, \forall i, j \in \mathcal{N}_{\text{EPG}}, \forall ij \in \ell_{\text{EPG}}. \quad (4)$$

We take the linearized DistFlow model to formulate power flow constraint on DN side, considering that power loss is usually much smaller than the power flow on the feeder for DN [13].

$$\begin{cases} p_i = \sum_j p_{ij} - p_{hi} \\ q_i = \sum_j q_{ij} - q_{hi} \\ u_i - u_j = 2(r_{ij} p_{ij} + x_{ij} q_{ij}) \end{cases},$$

$$\forall i, j \in \mathcal{N}_{\text{DN}}, \forall ij, hi \in \ell_{\text{DN}}, \forall h \in \mathcal{F}_i, \forall j \in \mathcal{D}_i. \quad (5)$$

It should be noted that SOC relaxation on the DistFlow model is also a widely adopted method for formulating the

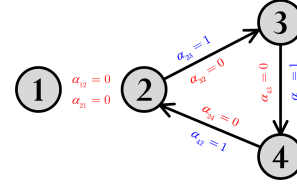


Fig. 1. Four-node network with a loop and an unconnected node.

convex power flow constraint [38]. It is still an open question whether the linearized DistFlow or the SOC relaxed DistFlow is generally more accurate [39]. The reason why we here selected the linearized DistFlow formulation is presented in Appendix A.

### D. Radial Topology Constraint

DN should keep radial topology, and the corresponding constraint should be explicitly expressed. The spanning constraint proposed in [14] is shown as follows:

$$0 \leq \alpha_{ij} + \alpha_{ji} \leq 1, \forall i, j \in \mathcal{N}_{\text{DN}}, \quad (6a)$$

$$\sum_i \alpha_{ij} = 1, \forall ij \in \ell_{\text{DN}}, \forall i \in \mathcal{F}_i, i \neq 1, \quad (6b)$$

$$\alpha_{j1} = 0, \forall j1 \in \ell_{\text{DN}}, \quad (6c)$$

where  $\alpha_{ij} \in \{0, 1\}$  is a binary variable used to indicate the link status for branches. For example,  $\alpha_{23} = 0$  means branch #23 is open and  $\alpha_{23} = 1$  means branch#23 is linked with flowing from node#2 to node#3. Equation (6a) regulates that the power flow direction on branch  $ij$  is unique. Equation (6b) requires that every node except the root node (marked with #1) has a unique father node. Equation (6c) implies that the root node has no father node.

Although (6) have been widely used in optimal DN reconfiguration, we find that they are insufficient to guarantee the radial topology for DN. As illustrated in Fig. 1, the set of  $\alpha_{ij}$  is satisfied with (6). However, it should be noted that this four-node network is not radial but with a loop and an unconnected node. It implies that if potential loops can be searched and eliminated in advance, the radial topology for DN can be guaranteed. Accordingly, the constraint that can prevent loop generation is required, as shown below:

$$0 \leq \sum_{ij} \alpha_{ij} + \alpha_{ji} \leq N_{\text{loop}} - 1, \forall ij \in \ell_{\text{loop}}, \quad (7)$$

where  $N_{\text{loop}}$  denotes the node number owned by a potential loop and  $\ell_{\text{loop}}$  denotes the set of branches in the potential loop. For a loop, the node number must equal the branch number. Therefore, if (7) holds, potential loops cannot exist. Once DN network is represented with help of graph theory, various of search algorithms like depth-first search and breadth-first search [40] can be used to find potential loops in DN topology.

In addition, with the introduction of  $\alpha_{ij}$ , the voltage drop term  $u_i - u_j = 2(r_{ij} p_{ij} + x_{ij} q_{ij})$  in (5) should be reformulated as

below with big-M relaxation:

$$\begin{cases} -M\alpha_{ij} \leq p_{ij} \leq M\alpha_{ij} \\ -M\alpha_{ij} \leq q_{ij} \leq M\alpha_{ij} \\ (u_i - k_{ij}) - (u_j - t_{ij}) = 2(r_{ij}p_{ij} + x_{ij}q_{ij}) \\ u_i^{\min}(1 - \alpha_{ij}) \leq k_{ij} \leq u_i^{\max}(1 - \alpha_{ij}) \\ u_j^{\min}(1 - \alpha_{ij}) \leq t_{ij} \leq u_j^{\max}(1 - \alpha_{ij}) \\ u_i^{\min}\alpha_{ij} \leq u_i - k_{ij} \leq u_i^{\max}\alpha_{ij} \\ u_j^{\min}\alpha_{ij} \leq u_j - t_{ij} \leq u_j^{\max}\alpha_{ij} \end{cases}, \quad (8)$$

$$\forall i, j \in \mathcal{N}_{\text{DN}}, \forall ij \in \ell_{\text{DN}},$$

where (8) is used to ensure that the voltage drop term is active when  $\alpha_{ij} = 1$ .  $k_{ij}$  and  $t_{ij}$  are the auxiliary variables.

### E. OLTC Action Constraint

OLTC installed on the substation provides the voltage adjustment in the DN root voltage. In this case,  $u_i - u_j = 2(r_{ij}p_{ij} + x_{ij}q_{ij})$  in (5) can be rewritten as:

$$u_i - K_{\text{T}}u_j = 2(r_{ij}p_{ij} + x_{ij}q_{ij}), \forall i, j \in \mathcal{N}_{\text{DN}}, \forall ij \in \ell_{\text{DN}}. \quad (9)$$

Note that there is a bilinear term  $K_{\text{T}}u_j$  involved in (9). To handle  $K_{\text{T}}u_j$ , we assume that  $K_{\text{T}}$  takes a possible discrete value from the set  $\{k_{\text{T},1}, k_{\text{T},2}, \dots, k_{\text{T},N}\}$ , and  $K_{\text{T}}$  can be expressed with a series of binary auxiliary variables  $b_{\text{T},n} \in \{0, 1\}$ , such that:

$$\begin{cases} K_{\text{T}} = \sum_n k_{\text{T},n} b_{\text{T},n} \\ \sum_n b_{\text{T},n} = 1 \end{cases}, \forall n \in \{1, 2, \dots, N\}. \quad (10a)$$

We substitute (10a) into (9), then the bilinear term  $K_{\text{T}}u_j$  is generated, which can be further replaced by a series of auxiliary variables  $v_{\text{T},n}$  and are subject to big-M relaxation, such that:

$$\begin{cases} K_{\text{T}}u_j = \sum_n k_{\text{T},n} v_{\text{T},n} \\ u_j - M(1 - b_{\text{T},n}) \leq v_{\text{T},n} \leq u_j + M(1 - b_{\text{T},n}) \\ -Mb_{\text{T},n} \leq v_{\text{T},n} \leq Mb_{\text{T},n} \\ \sum_n b_{\text{T},n} = 1 \end{cases}, \quad (10b)$$

$$\forall n \in \{1, 2, \dots, N\}.$$

As shown in (10b),  $K_{\text{T}}u_j$  will eventually be equivalently formulated as a set of linear constraints with mixed integer variables, enabling compatibility with the mixed-integer convex optimization.

### F. LRG Capacity Constraint

Considering that LRG integrates into DN with PQ control mode, LRG has the capability of controllable power outputs. The original capacity constraint can be expressed as below:

$$0 \leq p_{i,\text{LRG}} \leq p_{i,\text{LRG}}^{\text{MPPT}}, \forall i \in \mathcal{N}_{\text{DN}}, \quad (11a)$$

$$p_{i,\text{LRG}}^2 + q_{i,\text{LRG}}^2 \leq (s_{i,\text{LRG}}^{\text{rated}})^2, \forall i \in \mathcal{N}_{\text{DN}}, \quad (11b)$$

where (11a) indicates that the active power output of LRG cannot exceed the available maximum power point tracking

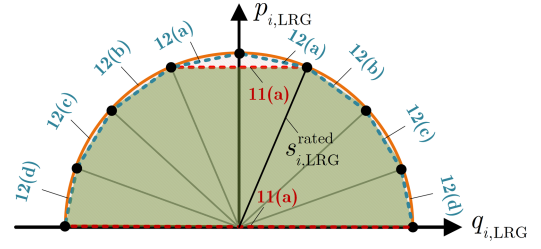


Fig. 2. Linearization of LRG capacity constraint. The green partition represents the available capacity of apparent power.

(MPPT) value. Equation (11b) forms a semicircle area related to the apparent power capacity of LRG, which requires a further transformation since it is nonlinear.

As shown in Fig. 2, the mentioned semicircle area can be approximated by a half of hexadecagon. In this way, (11b) can be further linearized by a set of linear constraint:

$$\left| \tan \frac{1}{16} \pi \times q_{i,\text{LRG}} \right| \leq s_{i,\text{LRG}}^{\text{rated}} - p_{i,\text{LRG}}, \forall i \in \mathcal{N}_{\text{DN}}, \quad (12a)$$

$$\begin{aligned} & \left| \tan \frac{3}{16} \pi \times q_{i,\text{LRG}} \right| \\ & \leq \left( \sin \frac{2}{8} \pi + \tan \frac{3}{16} \pi \cos \frac{2}{8} \pi \right) s_{i,\text{LRG}}^{\text{rated}} - p_{i,\text{LRG}}, \forall i \in \mathcal{N}_{\text{DN}}, \end{aligned} \quad (12b)$$

$$\begin{aligned} & \left| \tan \frac{5}{16} \pi \times q_{i,\text{LRG}} \right| \\ & \leq \left( \sin \frac{1}{8} \pi + \tan \frac{5}{16} \pi \cos \frac{1}{8} \pi \right) s_{i,\text{LRG}}^{\text{rated}} - p_{i,\text{LRG}}, \forall i \in \mathcal{N}_{\text{DN}}, \end{aligned} \quad (12c)$$

$$\left| \tan \frac{7}{16} \pi \times q_{i,\text{LRG}} \right| \leq \tan \frac{7}{16} \pi s_{i,\text{LRG}}^{\text{rated}} - p_{i,\text{LRG}}, \forall i \in \mathcal{N}_{\text{DN}}, \quad (12d)$$

where the combination of (12a)–(12d) along with (11a) formulates a set of linear LRG capacity constraints.

### G. LDC Function Constraint

LDC with  $q(u)$  type [21] is depicted in Fig. 3, and it distinguishes dead-band zone, droop zone, and saturation zone:

$$q_{i,\text{LRG}} = \begin{cases} q_{i,\text{LRG}}^{\text{def}} - \kappa_i^{\text{left}} (u_i - u_{i,\text{DB}}^{\min}), & u_i^{\min} \leq u_i < u_{i,\text{DB}}^{\min} \\ q_{i,\text{LRG}}^{\text{def}}, & u_{i,\text{DB}}^{\min} \leq u_i \leq u_{i,\text{DB}}^{\max} \\ q_{i,\text{LRG}}^{\text{def}} + \kappa_i^{\text{right}} (u_i - u_{i,\text{DB}}^{\max}), & u_{i,\text{DB}}^{\max} < u_i \leq u_i^{\max} \end{cases}, \quad (13a)$$

$$\forall i \in \mathcal{N}_{\text{DN}},$$

$$q_{i,\text{LRG}}^{\text{sat},\min} \leq q_{i,\text{LRG}} \leq q_{i,\text{LRG}}^{\text{sat},\max}, \forall i \in \mathcal{N}_{\text{DN}}, \quad (13b)$$

$$q_{i,\text{LRG}}^{\text{sat},\min} \leq q_{i,\text{LRG}}^{\text{def}} \leq q_{i,\text{LRG}}^{\text{sat},\max}, \forall i \in \mathcal{N}_{\text{DN}}, \quad (13c)$$

$$\begin{cases} q_{i,\text{LRG}}^{\text{sat},\max}, & u_i \geq u_i^{\min} \\ q_{i,\text{LRG}}^{\text{sat},\min}, & u_i \leq u_i^{\max} \end{cases}, \forall i \in \mathcal{N}_{\text{DN}}, \quad (13d)$$

$$\begin{cases} q_{i,\text{LRG}}^{\text{sat},\max}, & u_i \geq u_i^{\text{ind}} \\ q_{i,\text{LRG}}^{\text{sat},\min}, & u_i \leq u_i^{\text{cap}} \end{cases}, \forall i \in \mathcal{N}_{\text{DN}}, \quad (13e)$$

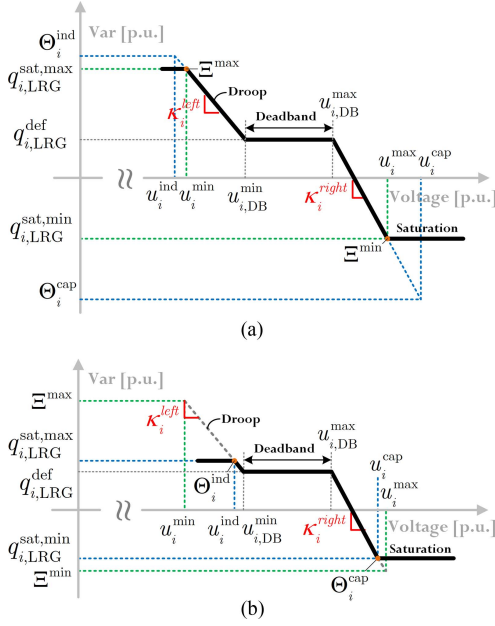


Fig. 3. LDC curve for LRG. (a) Corresponds to the condition that the available reactive power capacity of LRG is abundant. (b) Corresponds to the condition that the available reactive power capacity of LRG is insufficient.

$$\begin{cases} u_i^{\min} \geq u_i^{\text{ind}} \\ u_i^{\max} \leq u_i^{\text{cap}} \end{cases}, \forall i \in \mathcal{N}_{\text{DN}}, \quad (13f)$$

$$\begin{cases} u_i^{\min} \leq u_i^{\text{ind}} \\ u_i^{\max} \geq u_i^{\text{cap}} \end{cases}, \forall i \in \mathcal{N}_{\text{DN}}, \quad (13g)$$

where (13a)–(13c) are common constraints that depict the LDC curve shown in both Fig. 3(a) and (b). Equation (13a) regulates that when the measured local voltage is located within the dead-band zone  $[u_{i,\text{DB}}^{\min}, u_{i,\text{DB}}^{\max}]$ , the reactive power output of LRG keeps the optimized default value  $q_{i,\text{LRG}}^{\text{def}}$  unchanged. Once the measured local voltage is out of  $[u_{i,\text{DB}}^{\min}, u_{i,\text{DB}}^{\max}]$ , real-time voltage adjustment is activated according to the LDC curve with parameters  $\kappa_i^{\text{left}}$  and  $\kappa_i^{\text{right}}$ . It is clear to observe that (13b) and (13c) hold for both Fig. 3(a) and (b). Equations (13d) and (13f) are specific constraints for Fig. 3(a), which indicates that if the measured local voltage violates  $[u_i^{\min}, u_i^{\max}]$ , the reactive power output reaches saturation  $q_{i,\text{LRG}}^{\text{sat},\min}/\text{max}$ . Equations (13e) and (13g) are specific constraints for Fig. 3(b), which indicates that if the measured local voltage violates  $[u_i^{\text{cap}}, u_i^{\text{ind}}]$ , the reactive power output reaches the saturation  $q_{i,\text{LRG}}^{\text{sat},\min}/\text{max}$ . Note that  $q_{i,\text{LRG}}^{\text{sat},\min}$  and  $q_{i,\text{LRG}}^{\text{sat},\max}$  are affected by the available reactive power capacity of LRG, which are defined as:

$$\Theta_i^{\text{cap}} := -\sqrt{(s_{i,\text{LRG}}^{\text{rated}})^2 - p_{i,\text{LRG}}^2}, \forall i \in \mathcal{N}_{\text{DN}}, \quad (14a)$$

$$\Theta_i^{\text{ind}} := +\sqrt{(s_{i,\text{LRG}}^{\text{rated}})^2 - p_{i,\text{LRG}}^2}, \forall i \in \mathcal{N}_{\text{DN}}. \quad (14b)$$

Also, we defined the bounds associated with  $u_i^{\min}$  and  $u_i^{\max}$  as:

$$\Xi_i^{\min} := q_{i,\text{LRG}}^{\text{def}} - \kappa_i^{\text{left}} (u_i^{\min} - u_{i,\text{DB}}^{\min}), \forall i \in \mathcal{N}_{\text{DN}}, \quad (15a)$$

$$\Xi_i^{\max} := q_{i,\text{LRG}}^{\text{def}} + \kappa_i^{\text{right}} (u_i^{\max} - u_{i,\text{DB}}^{\max}), \forall i \in \mathcal{N}_{\text{DN}}. \quad (15b)$$

As shown in Fig. 3(a), when the available reactive power of capacities of LRG is abundant, i.e.,  $[\Theta_i^{\text{cap}}, \Theta_i^{\text{ind}}]$  is wider than  $[\Xi_i^{\min}, \Xi_i^{\max}]$ ,  $q_{i,\text{LRG}}^{\text{sat},\min}$  and  $q_{i,\text{LRG}}^{\text{sat},\max}$  are determined as:

$$q_{i,\text{LRG}}^{\text{sat},\min} = \Xi_i^{\min}, \Xi_i^{\min} \geq \Theta_i^{\text{cap}}, \forall i \in \mathcal{N}_{\text{DN}}, \quad (16a)$$

$$q_{i,\text{LRG}}^{\text{sat},\max} = \Xi_i^{\max}, \Xi_i^{\max} \leq \Theta_i^{\text{ind}}, \forall i \in \mathcal{N}_{\text{DN}}. \quad (16b)$$

Otherwise, as shown in Fig. 3(b)  $q_{i,\text{LRG}}^{\text{sat},\min}$  and  $q_{i,\text{LRG}}^{\text{sat},\max}$  are determined as:

$$q_{i,\text{LRG}}^{\text{sat},\min} = \Theta_i^{\text{cap}}, \Xi_i^{\min} \leq \Theta_i^{\text{cap}}, \forall i \in \mathcal{N}_{\text{DN}}, \quad (17a)$$

$$q_{i,\text{LRG}}^{\text{sat},\max} = \Theta_i^{\text{ind}}, \Xi_i^{\max} \geq \Theta_i^{\text{ind}}, \forall i \in \mathcal{N}_{\text{DN}}. \quad (17b)$$

Looking back (13a), due to the voltage security constraint that  $u_i^{\min} \leq u_i \leq u_i^{\max}$ , as long as the constructed OPF model has feasible solutions, (13a) always holds under a specific condition that  $(q_{i,\text{LRG}}^*, q_{i,\text{LRG}}^{\text{def}}, u_{i,\text{LRG}}^*)$ , and appropriate  $(q_{i,\text{LRG}}^{\text{sat},\min*}, q_{i,\text{LRG}}^{\text{sat},\max*})$  can definitely be found that makes (13b) and (13c) hold. In this case,  $u_i^{\text{cap}/\text{ind}}$ ,  $\Xi_i^{\min}/\text{max}$ , and  $\Theta_i^{\text{cap}/\text{ind}}$  can be treated as slack variables, and (13d)–(13g) and (16)–(17) naturally hold and become redundant for forming the LDC function in both Fig. 3(a) and (b). Notably,  $q_{i,\text{LRG}}^{\text{sat},\min}$  and  $q_{i,\text{LRG}}^{\text{sat},\max}$  should subject to the constraints below:

$$p_{i,\text{LRG}}^2 + (q_{i,\text{LRG}}^{\text{sat},\min})^2 \leq (s_{i,\text{LRG}}^{\text{rated}})^2, \forall i \in \mathcal{N}_{\text{DN}}, \quad (18a)$$

$$p_{i,\text{LRG}}^2 + (q_{i,\text{LRG}}^{\text{sat},\max})^2 \leq (s_{i,\text{LRG}}^{\text{rated}})^2, \forall i \in \mathcal{N}_{\text{DN}}, \quad (18b)$$

where nonlinear (18a) and (18b) can be further approximated as a series of linear constraints, which are similar to (12a)–(12d). According to the above, LDC curve in Fig. 3(a) and (b) can be generalized formulated via (13a)–(13c) and (18).

Subsequently, for handling (13a) with conditional function, we introduce auxiliary variables  $f_{i,1}$ ,  $f_{i,2}$ ,  $f_{i,3}$  as follows:

$$f_{i,1} := q_{i,\text{LRG}}^{\text{def}} - \kappa_i^{\text{left}} (u_i - u_{i,\text{DB}}^{\min}), u_i^{\min} \leq u_i < u_{i,\text{DB}}^{\min} \\ \forall i \in \mathcal{N}_{\text{DN}}, \quad (19a)$$

$$f_{i,2} := q_{i,\text{LRG}}^{\text{def}}, u_{i,\text{DB}}^{\min} \leq u_i \leq u_{i,\text{DB}}^{\max} \\ \forall i \in \mathcal{N}_{\text{DN}}, \quad (19b)$$

$$f_{i,3} := q_{i,\text{LRG}}^{\text{def}} + \kappa_i^{\text{right}} (u_i - u_{i,\text{DB}}^{\max}), u_{i,\text{DB}}^{\max} < u_i \leq u_i^{\max} \\ \forall i \in \mathcal{N}_{\text{DN}}. \quad (19c)$$

Based on (19),  $q_{i,\text{LRG}}$  can be equivalently expressed as a combination of binary variables  $\chi_{i,n} \in \{0, 1\}$ , such that:

$$\begin{cases} q_{i,\text{LRG}} = \sum_n \chi_{i,n} f_{i,n} \\ \sum_n \chi_{i,n} = 1, \end{cases}, n \in \{1, 2, 3\}, \forall i \in \mathcal{N}_{\text{DN}}, \quad (20a)$$

$$[\chi_{i,1}, \chi_{i,2}, \chi_{i,3}] \\ = \begin{cases} [1, 0, 0], u_i^{\min} \leq u_i < u_{i,\text{DB}}^{\min} \\ [0, 1, 0], u_{i,\text{DB}}^{\min} \leq u_i \leq u_{i,\text{DB}}^{\max} \\ [0, 0, 1], u_{i,\text{DB}}^{\max} < u_i \leq u_i^{\max} \end{cases}, \forall i \in \mathcal{N}_{\text{DN}}. \quad (20b)$$

The bilinear term  $\chi_{i,n}f_{i,n}$  can be further expressed with the additional auxiliary variables  $w_{i,n}$ , such that:

$$q_{i,\text{LRG}} = \sum_n w_{i,n}, \quad n = 1, 2, 3, \quad \forall i \in \mathcal{N}_{\text{DN}}, \quad (21a)$$

$$\begin{cases} q_{i,\text{LRG}}^{\text{sat},\text{min}} \chi_{i,n} \leq w_{i,n} \leq q_{i,\text{LRG}}^{\text{sat},\text{max}} \chi_{i,n} \\ f_{i,n} + q_{i,\text{LRG}}^{\text{sat},\text{min}} (1 - \chi_{i,n}) \leq w_{i,n} \leq f_{i,n} \\ \quad + q_{i,\text{LRG}}^{\text{sat},\text{max}} (1 - \chi_{i,n}) \end{cases}, \quad (21b)$$

$$n \in \{1, 2, 3\}, \quad \forall i \in \mathcal{N}_{\text{DN}}.$$

Note that bilinear terms  $q_{i,\text{LRG}}^{\text{sat},\text{min}} \chi_{i,n}$  and  $q_{i,\text{LRG}}^{\text{sat},\text{max}} \chi_{i,n}$  are successively generated in (21b). For handling them, the additional sets of auxiliary variables  $\tau_{i,n}$  and  $\sigma_{i,n}$  are introduced to replace  $q_{i,\text{LRG}}^{\text{sat},\text{min}} \chi_{i,n}$  and  $q_{i,\text{LRG}}^{\text{sat},\text{max}} \chi_{i,n}$  via big-M relaxation, which yields the following:

$$\begin{cases} -M\chi_{i,n} \leq \sigma_{i,n} \leq M\chi_{i,n} \\ -M(1 - \chi_{i,n}) \leq \sigma_{i,n} - q_{i,\text{LRG}}^{\text{sat},\text{min}} \leq M(1 - \chi_{i,n}) \end{cases}, \quad (22a)$$

$$n \in \{1, 2, 3\}, \quad \forall i \in \mathcal{N}_{\text{DN}},$$

$$\begin{cases} -M\chi_{i,n} \leq \tau_{i,n} \leq M\chi_{i,n} \\ -M(1 - \chi_{i,n}) \leq \tau_{i,n} - q_{i,\text{LRG}}^{\text{sat},\text{max}} \leq M(1 - \chi_{i,n}) \end{cases}, \quad (22b)$$

$$n \in \{1, 2, 3\}, \quad \forall i \in \mathcal{N}_{\text{DN}}.$$

Besides, voltage conditions in (20b) can be explicitly expressed as follows with big-M relaxation:

$$\begin{cases} -M(1 - \chi_{i,1}) \leq u_i - u_i^{\text{min}} \\ u_i - (u_{i,\text{DB}}^{\text{min}} - \varepsilon) \leq M(1 - \chi_{i,1}) \end{cases}, \quad \forall i \in \mathcal{N}_{\text{DN}}, \quad (23a)$$

$$\begin{cases} -M(1 - \chi_{i,2}) \leq u_i - u_{i,\text{DB}}^{\text{min}} \\ u_i - u_{i,\text{DB}}^{\text{max}} \leq M(1 - \chi_{i,2}) \end{cases}, \quad \forall i \in \mathcal{N}_{\text{DN}}, \quad (23b)$$

$$\begin{cases} -M(1 - \chi_{i,3}) \leq u_i - (u_{i,\text{DB}}^{\text{min}} + \varepsilon) \\ u_i - u_i^{\text{max}} \leq M(1 - \chi_{i,3}) \end{cases}, \quad \forall i \in \mathcal{N}_{\text{DN}}, \quad (23c)$$

where  $\varepsilon$  has a tiny positive value and it is utilized to convert inequality “<” existing in (20b) to “≤”, to meet the standard form of an inequality constraint.

#### H. Other Constraints

The capacity constraint for generating system that  $p_{i,\text{G}}^2 + q_{i,\text{G}}^2 \leq (s_{i,\text{LRG}}^{\text{rated}})^2$  is also included. It can be formulated as similar to LRG capacity constraint as (12a)–(12d) by replacing  $p_{i,\text{LRG}}$ ,  $q_{i,\text{LRG}}$ ,  $s_{i,\text{LRG}}^{\text{rated}}$  with  $p_{i,\text{G}}$ ,  $q_{i,\text{G}}$ ,  $s_{i,\text{G}}^{\text{rated}}$ . Moreover, the power factor constraint for the generating system should also be added:

$$-p_{i,\text{G}} \tan(\cos^{-1}(\varphi_i^{\text{cap}})) \leq q_{i,\text{G}} \leq p_{i,\text{G}} \tan(\cos^{-1}(\varphi_i^{\text{ind}})), \quad \forall i \in \mathcal{N}_{\text{EPG}}. \quad (24)$$

### III. DISTRIBUTED OPTIMIZATION METHODS BASED ON THE AUGMENTED LAGRANGIAN RELAXATION

Considering the computation burden for global optimization and data privacy protection between EPG and DN, the distributed

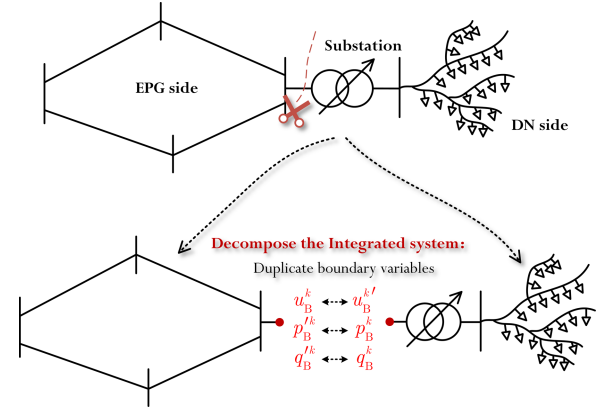


Fig. 4. Illustration of decomposing the integrated system of EPG and DN.

optimization methods based on the augmented Lagrangian relaxation are employed to solve the aforementioned OPF model via the boundary information exchanges between EPG and DN.

#### A. Model Decomposition and Distributed Solving

As shown in Fig. 4, by duplicating the boundary node, the boundary variables  $u_B$ ,  $p_B$  and  $q_B$  are generated. We use the superscript ( $'$ ) to represent the corresponding duplication variables.

Denote  $\mathbf{X}_B^{\text{EPG}} := [u_B, p'_B, q'_B]$  as the boundary variables on the EPG side and  $\mathbf{X}_B^{\text{DN}} := [u'_B, p_B, q_B]$  as the boundary variables on the DN side. The solving process of the distributed optimization methods based on the augmented Lagrangian relaxation is formulated as follows:

$$\widehat{\mathbf{X}}_B^{\text{EPG}} \in \arg \min \mathcal{L}_{\text{EPG}} \left( \mathbf{X}_B^{\text{EPG}}, \mathbf{X}_I^{\text{EPG}}, \widehat{\mathbf{X}}_B^{\text{DN}}, \widehat{\mathbf{l}} \right), \quad (25a)$$

$$\widehat{\mathbf{X}}_B^{\text{DN}} \in \arg \min \mathcal{L}_{\text{DN}} \left( \mathbf{X}_B^{\text{DN}}, \mathbf{X}_I^{\text{DN}}, \widehat{\mathbf{X}}_B^{\text{EPG}}, \widehat{\mathbf{l}} \right), \quad (25b)$$

$$\widehat{\mathbf{l}} \in \mathcal{M} \left( \widehat{\mathbf{X}}_B^{\text{DN}}, \widehat{\mathbf{X}}_B^{\text{EPG}}, \mathbf{l} \right), \quad (25c)$$

where the top mark ( $\widehat{\cdot}$ ) represents the determined value after distributed optimization.  $\mathbf{X}_I^{\text{EPG}} := [p_{i,\text{G}}, q_{i,\text{G}}]$  represents independent optimization variables on the EPG side, involving the active and reactive power outputs from generating systems.  $\mathbf{X}_I^{\text{DN}} := [p_{i,\text{LRG}}, q_{i,\text{LRG}}, \alpha_{ij}, K_T]$  represents independent optimization variables on the DN side, involving the active and reactive power outputs from LRG, link status of branches, and tap positions for OLTC.  $\mathbf{l} := [\lambda, \rho]$  includes Lagrangian multipliers  $\lambda$  and the penalty coefficient  $\rho$ .  $\mathcal{M}(\cdot)$  represents the iteration approach for Lagrangian multipliers and the penalty coefficient. Variables in bold represent their corresponding vector form.

The augmented Lagrangian relaxation is the upgrade of the Lagrangian relaxation with an extra quadratic penalty term for better convergence property. Three approaches, i.e., ATC, ADMM, and APP, are employed in this article. Regarding (25a) and (25b), ADMM and ATC have a unified expression, such that:

$$\min \mathcal{L}_{\text{EPG}}^{(k+1)} := f_{\text{EPG}} + \lambda^{(k)} \left( \mathbf{X}_B^{\text{EPG}} - \mathbf{X}_B^{\text{DN}(k)} \right)^T$$

$$+ \left\| \frac{1}{2} \rho^{(k)} \left( \mathbf{X}_B^{\text{EPG}} - \mathbf{X}_B^{\text{DN}(k)} \right) \right\|_2^2$$

s.t. (2a), (4), (24),

$$\min \mathcal{L}_{\text{DN}}^{(k+1)} := f_{\text{DN}} + \boldsymbol{\lambda}^{(k)} \left( \mathbf{X}_B^{\text{EPG}(k+1)} - \mathbf{X}_B^{\text{DN}} \right)^\top$$

$$+ \left\| \frac{1}{2} \rho^{(k)} \left( \mathbf{X}_B^{\text{EPG}(k+1)} - \mathbf{X}_B^{\text{DN}} \right) \right\|_2^2$$

s.t. (2b), (5) – (23),

where the superscript  $()^{(k)}$  represents the determined value at the  $k$ th iteration and the superscript  $()^\top$  represents the transpose of a matrix.

APP has a distinctive expression concerning (25a) and (25b), such that:

$$\min \mathcal{L}_{\text{EPG}}^{(k+1)} := f_{\text{EPG}} + \boldsymbol{\lambda}^{(k)} \mathbf{X}_B^{\text{EPG}\top}$$

$$+ \rho^{(k)} \left( \mathbf{X}_B^{\text{EPG}(k)} - \mathbf{X}_B^{\text{DN}(k)} \right) \mathbf{X}_B^{\text{EPG}\top}$$

$$+ \left\| \rho^{(k)} \left( \mathbf{X}_B^{\text{EPG}} - \mathbf{X}_B^{\text{EPG}(k)} \right) \right\|_2^2$$

s.t. (2a), (4), (24),

$$\min \mathcal{L}_{\text{DN}}^{(k+1)} := f_{\text{DN}} - \boldsymbol{\lambda}^{(k)} \mathbf{X}_B^{\text{DN}\top}$$

$$- \rho^{(k)} \left( \mathbf{X}_B^{\text{EPG}(k)} - \mathbf{X}_B^{\text{DN}(k)} \right) \mathbf{X}_B^{\text{DN}\top}$$

$$+ \left\| \rho^{(k)} \left( \mathbf{X}_B^{\text{DN}} - \mathbf{X}_B^{\text{DN}(k)} \right) \right\|_2^2$$

s.t. (2b), (5) – (23).

Regarding (25c), ADMM and APP have a unified expression, such that:

$$\mathcal{M} := \begin{cases} \boldsymbol{\lambda}^{(k+1)} \Leftarrow \boldsymbol{\lambda}^{(k)} + \rho^{(k)} \left( \mathbf{X}_B^{\text{EPG}(k+1)} - \mathbf{X}_B^{\text{DN}(k+1)} \right) \\ \rho^{(k+1)} \Leftarrow \rho^{(k)} \end{cases}.$$

ATC has a distinctive expression concerning (25c), such that:

$$\mathcal{M} := \begin{cases} \boldsymbol{\lambda}^{(k+1)} \Leftarrow \boldsymbol{\lambda}^{(k)} + \frac{1}{2} (\rho^{(k)})^2 \left( \mathbf{X}_B^{\text{EPG}(k+1)} - \mathbf{X}_B^{\text{DN}(k+1)} \right) \\ \rho^{(k+1)} \Leftarrow \gamma \rho^{(k)} \end{cases},$$

where  $\gamma > 1$  is used to adjust  $\rho$ .

### B. Parallel Processing

It can be found that, except for APP, the standard iteration process for ADMM and ATC is in serial. Equations (26a) and (26b) indicate that one is only available if the other is executed. Parallel processing is considered to address this issue [31], [41]. The parallel processing uses the average value of boundary variables on DN and EPG sides in every iteration. Comparing the processing flowchart illustrated in Fig. 5(a) and (b), we can see that EPG and DN can execute their local update simultaneously via the parallel processing approach, and the entire processing steps of one iteration can be reduced. In this way, the computation time required for one iteration is not the

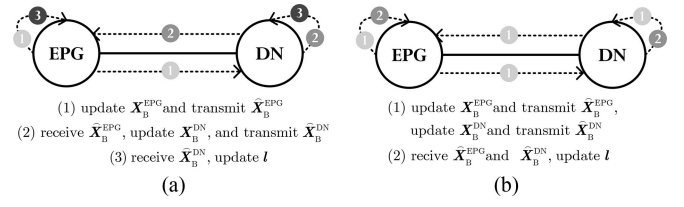


Fig. 5. Processing flow chart. (a) Represents the serial manner. (b) Represents the parallel manner.

sum of the computation time for EPG and DN but depends on one of them that takes a longer time.

Accordingly, (26a) and (26b) are transformed as:

$$\min \mathcal{L}_{\text{EPG}}^{(k+1)} :=$$

$$f_{\text{EPG}} + \boldsymbol{\lambda}_{\text{EPG}}^{(k)} \left( \mathbf{X}_B^{\text{EPG}} - \mathbf{X}_{\text{ave}}^{(k)} \right)^\top + \left\| \frac{1}{2} \rho^{(k)} \left( \mathbf{X}_B^{\text{EPG}} - \mathbf{X}_{\text{ave}}^{(k)} \right) \right\|_2^2$$

s.t. (2a), (4), (24),

$$\min \mathcal{L}_{\text{DN}}^{(k+1)} :=$$

$$f_{\text{DN}} + \boldsymbol{\lambda}_{\text{DN}}^{(k)} \left( \mathbf{X}_{\text{ave}}^{(k)} - \mathbf{X}_B^{\text{DN}} \right)^\top + \left\| \frac{1}{2} \rho^{(k)} \left( \mathbf{X}_{\text{ave}}^{(k)} - \mathbf{X}_B^{\text{DN}} \right) \right\|_2^2$$

s.t. (2b), (5) – (23),

$$\mathbf{X}_{\text{ave}}^{(k+1)} = \frac{1}{2} \left( \mathbf{X}_B^{\text{DN}(k)} + \mathbf{X}_B^{\text{EPG}(k)} \right).$$

Also, update process of Lagrangian multipliers in (28a) and (28b) are transformed as:

$$\begin{cases} \boldsymbol{\lambda}_{\text{EPG}}^{(k+1)} \Leftarrow \boldsymbol{\lambda}_{\text{EPG}}^{(k)} + \rho^{(k)} \left( \mathbf{X}_B^{\text{EPG}(k+1)} - \mathbf{X}_{\text{ave}}^{(k+1)} \right) \\ \boldsymbol{\lambda}_{\text{DN}}^{(k+1)} \Leftarrow \boldsymbol{\lambda}_{\text{DN}}^{(k)} + \rho^{(k)} \left( \mathbf{X}_{\text{ave}}^{(k+1)} - \mathbf{X}_B^{\text{DN}(k+1)} \right) \end{cases}, \quad (30a)$$

$$\begin{cases} \boldsymbol{\lambda}_{\text{EPG}}^{(k+1)} \Leftarrow \boldsymbol{\lambda}_{\text{EPG}}^{(k+1)} + \frac{1}{2} (\rho^{(k)})^2 \left( \mathbf{X}_B^{\text{EPG}(k+1)} - \mathbf{X}_{\text{ave}}^{(k+1)} \right) \\ \boldsymbol{\lambda}_{\text{DN}}^{(k+1)} \Leftarrow \boldsymbol{\lambda}_{\text{DN}}^{(k+1)} + \frac{1}{2} (\rho^{(k)})^2 \left( \mathbf{X}_{\text{ave}}^{(k+1)} - \mathbf{X}_B^{\text{DN}(k+1)} \right) \end{cases}.$$

Moreover, while APP already been taken the parallel iteration process, it can also be transformed into an average consensus-based parallel iteration process. The approach is similar to (29), which replaces  $\mathbf{X}_B^{\text{DN}(k)}$  and  $\mathbf{X}_B^{\text{EPG}(k)}$  in (27a) and (27b) with  $\mathbf{X}_{\text{ave}}^{(k)}$ , respectively.

### C. Asynchronous Implementation

In practice, implementing distributed optimization methods based on the augmented Lagrangian relaxation might encounter the challenge of time delay. When time delay is considered, there are two types of ways to implement distributed optimization, i.e., synchronous and asynchronous. In particular, an asynchronous optimization framework based on ADMM has been proposed in [42], [43], which can be extended and applied to other augmented Lagrangian relaxation-based distributed optimization methods.

As presented in Fig. 6, assume that there are one EPG and two DNs that take different times to execute optimization tasks.

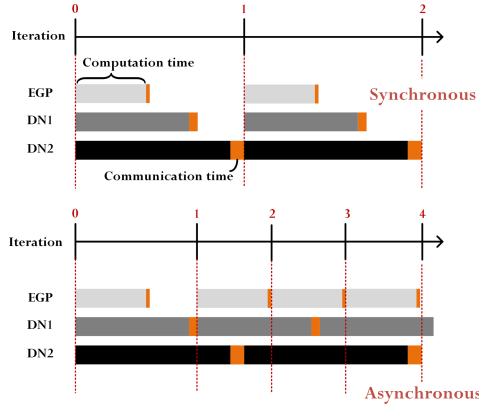


Fig. 6. Illustration of the synchronous and asynchronous implementation.

Under the synchronous protocol, only when all two DNs have completed the update and EPG has received all the boundary information from DNs, (29c) and (30) can be executed. In contrast, the asynchronous protocol requires only one DN to complete the update in one iteration. If EPG receives half boundary information from DNs, then (29c) and (30) are executed. During the same period, the distributed optimization under the asynchronous protocol can complete more iterations than it under synchronous protocol.

Define  $\mathcal{R}$  as the DN set, and its boundary information have been received by EPG.  $\bar{\mathcal{R}}$  denotes the complementary set of  $\mathcal{R}$ . We use subscript  $(\cdot)_{\tau}$  to represent DN#  $\tau$  among the DN set. Then we have the modified update formulation regarding boundary variables that match the asynchronous protocol, such that:

$$\mathbf{X}_{B,\tau}^{\text{DN}(k+1)} \leftarrow \begin{cases} \mathbf{X}_{B,\tau}^{\text{DN}(k)}, \forall \tau \in \bar{\mathcal{R}} \\ \mathbf{X}_{B,\tau}^{\text{DN}(k+1)} \in \arg \min(29b), \forall \tau \in \mathcal{R} \end{cases}, \quad (31a)$$

$$\mathbf{X}_{\text{ave},\tau}^{(k+1)} \leftarrow \begin{cases} \mathbf{X}_{\text{ave},\tau}^{(k)}, \forall \tau \in \bar{\mathcal{R}} \\ \frac{1}{2} \left( \mathbf{X}_{B,\tau}^{\text{DN}(k)} + \mathbf{X}_{B,\tau}^{\text{EPG}(k)} \right), \forall \tau \in \mathcal{R} \end{cases}. \quad (31b)$$

#### D. Remarks

Firstly, reviewing (1)–(24), we can see that the constructed OPF model concerning DN reconfiguration is not purely convex due to the integer variables involved. In this case, optimality and convergence cannot be rigorous guaranteed when applying the augmented Lagrangian relaxation-based distributed optimization methods. Fortunately, we found that there have been several attempts indicating that the augmented Lagrangian relaxation-based distributed optimization methods can still be taken to solve nonconvex OPF problems [44], [45], [46]. Although the optimization results for nonconvex problems are not as good as those for convex problems, they are still acceptable. As a result, this article attempts to solve the constructed mix-integer convex OPF model involving DN reconfiguration using ATC, ADMM, and APP. The residuals are used as the iteration-stopping criterion, such that:

$$\varepsilon_p^{(k)} := \frac{1}{D} \|\mathbf{X}_B^{\text{EPG}(k)} - \mathbf{X}_B^{\text{DG}(k)}\|_2, \quad (32a)$$

$$\varepsilon_d^{(k)} := \frac{1}{D} \|\mathbf{X}_B^{\text{EPG}(k+1)} - \mathbf{X}_B^{\text{EPG}(k)}\|_2. \quad (32b)$$

Then as shown in Fig. 3, LDC is described as  $q(u)$  type, which is squared in the local voltage amplitude [21] and origins from the conventional version, i.e.,  $q(v)$  type. Besides,  $q(v)$  type has other modified versions, such as the simplified  $q(v)$  type without dead-band and the delayed  $q_t(v_t, q_{t-1})$  type reading the current local voltage and the previous reactive power output [22], [23]. We would like to address that only minor modification is needed, and the proposed OPF model can be compatible with the conventional  $q(v)$  type. More details can be found in Appendix B.

#### IV. EXTREME SCENARIO METHOD

The uncertainty related to LRG integration stems from the available MPPT power, which heavily affects the decision-making in optimal DN reconfiguration. To address this challenge, the extreme scenario method is introduced.

##### A. Two-Stage Decision-Making

In practice, devices for DN reconfiguration are scheduled under different timescales since they have different response speeds. Therefore, the proposed OPF model (1)–(24) can be described as a standard two-stage decision-making problem with the below general form:

$$\begin{aligned} & \min f(\boldsymbol{\xi}_{(s)}, \mathbf{x}_{(s)}, \mathbf{y}_{(s)}) \\ & \text{s.t.} \begin{cases} \mathcal{G}(\boldsymbol{\xi}_{(s)}, \mathbf{x}_{(s)}, \mathbf{y}_{(s)}) \leq 0 \\ \mathcal{H}(\boldsymbol{\xi}_{(s)}, \mathbf{x}_{(s)}, \mathbf{y}_{(s)}) = 0 \end{cases} \\ & \forall s \in \mathcal{S}, \end{aligned} \quad (33)$$

where the subscript  $(\cdot)_{(s)}$  corresponds to the parameters and variables in uncertain scenario#  $s$ .  $\mathcal{S}$  denotes the set that covers all uncertain scenarios. The uncertainty related to LRG origins from the available MPPT power, i.e.,  $\boldsymbol{\xi}_{(s)} := \mathbf{p}_{i,\text{LRG},(s)}^{\text{MPPT}} \cdot \mathbf{y}_{(s)}$  represents the variables linked with slow-response devices, including power outputs of generating systems in EPG, tap positions of OLTC in DN, and link status of branches in DN, i.e.,  $\mathbf{y}_{(s)} := [\mathbf{p}_{i,\text{G},(s)}, \mathbf{q}_{i,\text{G},(s)}, K_{\text{T},(s)}, \boldsymbol{\alpha}_{ij,(s)}]$ .  $\mathbf{x}_{(s)}$  represents the variables linked with fast-response devices, including power outputs of LRG in DN, i.e.,  $\mathbf{x}_{(s)} := [\mathbf{p}_{i,\text{LRG},(s)}, \mathbf{q}_{i,\text{LRG},(s)}]$ .

A robust two-stage decision-making means the condition holds that the robust  $\mathbf{y}_{(s)}$  (i.e.,  $\mathbf{y}_{(1)} = \mathbf{y}_{(2)} = \dots = \mathbf{y}_{(\text{Num}(\mathcal{S}))}$ ) are determined in the first stage, and then a feasible  $\mathbf{x}_{(s)}$  is definitely found in the second stage for arbitrary  $\boldsymbol{\xi}_{(s)}$ . In this case, a robust formulation of (33) is formed as:

$$\begin{aligned} & \min \sum_s f(\boldsymbol{\xi}_{(s)}, \mathbf{x}_{(s)}, \mathbf{y}) \\ & \text{s.t.} \begin{cases} \mathcal{G}(\boldsymbol{\xi}_{(s)}, \mathbf{x}_{(s)}, \mathbf{y}) \leq 0 \\ \mathcal{H}(\boldsymbol{\xi}_{(s)}, \mathbf{x}_{(s)}, \mathbf{y}) = 0 \end{cases} \\ & \forall s \in \mathcal{S}. \end{aligned} \quad (34)$$

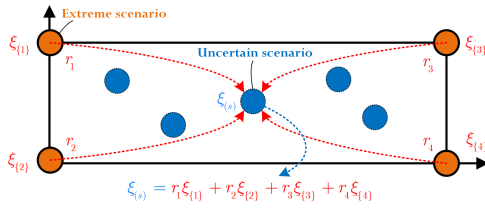


Fig. 7. Schematic diagram of the relationship between extreme and uncertain scenarios. The dimension of the uncertain variable is assumed to be 2.

where  $\mathbf{y}$  served as the “here-and-now” decision that cannot be adjusted after the uncertainty  $\xi_{(s)}$  is revealed, while the “wait-and-see” decision  $\mathbf{x}_{(s)}$  can be adjusted following the actual  $\widehat{\xi}_{(s)}$ .

### B. Robustness of the Extreme Scenario Method

To guarantee the existence of feasible solutions in the second stage for (34), an intuitive approach is to take all uncertain scenarios into account and list the corresponding constraint, but it is prominent mass computing. Fortunately, it is not necessary to consider all uncertain scenarios. Because once the second-stage feasible solutions exist when confronted with extreme scenarios, (34) must have the second-stage feasible solutions for all uncertain scenarios, which is the essence of the extreme scenario method. The robustness of the extreme scenario method has been validated in [34], [35], [36], and the proof is presented as follows.

Firstly, an OPF problem considering extreme scenarios is formulated as below:

$$\begin{aligned} & \min \sum_e f(\xi_{\{e\}}, \mathbf{x}_{\{e\}}, \mathbf{y}) \\ & \text{s.t.} \begin{cases} \mathcal{G}(\xi_{\{e\}}, \mathbf{x}_{\{e\}}, \mathbf{y}) \leq 0 \\ \mathcal{H}(\xi_{\{e\}}, \mathbf{x}_{\{e\}}, \mathbf{y}) = 0 \end{cases} \\ & \forall e \in \mathcal{E}, \end{aligned} \quad (35)$$

where the subscript  $(\cdot)_{\{e\}}$  corresponds to the parameters and variables in extreme scenario#  $e$ .  $\mathcal{E}$  denotes the set that covers all extreme scenarios and obviously that  $\mathcal{E} \subseteq \mathcal{S}$ . As shown in Fig. 7, if  $\xi_{(s)}$  is a 2-dimensional variable, the number of  $\xi_{\{e\}}$  will be  $2^2 = 4$ . Given that  $\sum_e r_e = 1, r_e \geq 0$ , and it is clear that  $\xi_{(s)}$  corresponding to the arbitrary uncertain scenario can be expressed as  $\xi_{(s)} = \sum_e r_e \xi_{\{e\}}$ .

Then, what we should do is to prove that if constraints in (35) hold in all extreme scenarios  $\mathcal{E}$ , constraints in (33) definitely hold for all the uncertain scenarios  $\mathcal{S}$ . Review (2)–(24), constraints in (35) can be explicitly expressed as:

$$\mathcal{G}_1(\xi_{\{e\}}, \mathbf{x}_{\{e\}}, \mathbf{y}) := \mathbf{A}_G \xi_{\{e\}}^\top + \mathbf{B}_G \mathbf{x}_{\{e\}}^\top + \mathbf{C}_G \mathbf{y}^\top \leq 0, \quad (36a)$$

$$\mathcal{H}(\xi_{\{e\}}, \mathbf{x}_{\{e\}}, \mathbf{y}) := \mathbf{A}_H \xi_{\{e\}}^\top + \mathbf{B}_H \mathbf{x}_{\{e\}}^\top + \mathbf{C}_H \mathbf{y}^\top = 0, \quad (36b)$$

$$\mathcal{G}_2(\mathbf{x}_{\{e\}}) := \|\mathbf{E} \circ \mathbf{x}_{\{e\}}\|_2 - \mathbf{F} \mathbf{x}_{\{e\}}^\top \leq 0, \quad (36c)$$

where  $\mathbf{A}_{G/H}$ ,  $\mathbf{B}_{G/H}$ ,  $\mathbf{C}_{G/H}$ ,  $\mathbf{E}$ , and  $\mathbf{F}$  are the coefficient matrixes of constraints in (35).  $\circ$  denotes element-wise multiplication. Equations (36a) and (36b) corresponds to the linear equality and quality constraints among (2)–(24), respectively. Equation

(36c) corresponds to the SOC relaxation term in (4), thus only the second-stage variables  $\mathbf{x}_{\{e\}}$  are contained.

Based on (36a) and (36b), we have that:

$$\sum_e r_e \mathcal{G}_1(\xi_{\{e\}}, \mathbf{x}_{\{e\}}, \mathbf{y}) = \mathcal{G}_1 \left( \sum_e r_e \xi_{\{e\}}, \sum_e r_e \mathbf{x}_{\{e\}}, \mathbf{y} \right), \quad (37a)$$

$$\sum_e r_e \mathcal{H}(\xi_{\{e\}}, \mathbf{x}_{\{e\}}, \mathbf{y}) = \mathcal{H} \left( \sum_e r_e \xi_{\{e\}}, \sum_e r_e \mathbf{x}_{\{e\}}, \mathbf{y} \right). \quad (37b)$$

Clearly, if (36a) holds,  $\mathcal{G}_1(\sum_e r_e \xi_{\{e\}}, \sum_e r_e \mathbf{x}_{\{e\}}, \mathbf{y}) \leq 0$  and  $\mathcal{H}(\sum_e r_e \xi_{\{e\}}, \sum_e r_e \mathbf{x}_{\{e\}}, \mathbf{y}) \leq 0$  will hold.

For  $\mathcal{G}_2(\mathbf{x}_{\{e\}})$ , it is a hypo-convex function. With help of Jensen inequality [47], we have that:

$$\mathcal{G}_2 \left( \sum_e r_e \mathbf{x}_{\{e\}} \right) \leq \sum_e r_e \mathcal{G}_2(\mathbf{x}_{\{e\}}). \quad (38)$$

Hence, if (36c) holds,  $\mathcal{G}_2(\sum_e r_e \mathbf{x}_{\{e\}}) \leq 0$  will hold.

Moreover, it must hold that a  $\widehat{\mathbf{x}}$  inside the convex feasible region of (33) can be linearly expressed by the boundary point  $\mathbf{x}_{\{e\}}$ , which yields the following [48]:

$$\begin{cases} \widehat{\mathbf{x}} = \sum_e r_e \mathbf{x}_{\{e\}} \\ \widehat{\mathbf{x}} \in \{\mathbf{x}_{(1)}, \mathbf{x}_{(2)}, \dots, \mathbf{x}_{(Nums(\mathcal{S}))}\} \end{cases}. \quad (39)$$

Combining (35)–(39), it can be deduced that once  $\mathbf{y}$  in the first-stage decision-making makes (35) that covers all extreme scenarios  $\xi_{\{e\}}$  have feasible solutions  $\mathbf{x}_{\{e\}}$  in the second-stage decision-making, it can also make (34) that covers all uncertain scenarios  $\xi_{(s)}$  have feasible solutions  $\mathbf{x}_{(s)}$  in the second-stage decision-making.

### C. Application in the Distributed OPF Model

The extreme scenario method is intuitive and straightforward to be adopted. However, once multiple DNs are considered in the constructed distributed OPF model concerning DN reconfiguration, the number of extreme scenarios will be exponential growth as the number of uncertain variables associated with LRG increases. It is necessary to find an appropriate way to reach the application of the extreme scenario method in the proposed distributed OPF model to meet the requirements in the practical application better.

The core of the augmented Lagrangian relaxation-based distributed optimization methods is information exchanges regarding the boundary variables. If the boundary variables are compulsorily required to be equal in each extreme scenario, we have the modified version of (35) with a compulsory constraint, such that:

$$\begin{aligned} & \min \sum_e f(\xi_{\{e\}}, \mathbf{x}_{\{e\}}, \mathbf{y}) \\ & \text{s.t.} \begin{cases} \mathcal{G}(\xi_{\{e\}}, [\mathbf{x}'_{\{e\}}, \mathbf{z}_{\{e\}}], \mathbf{y}) \leq 0 \\ \mathcal{H}(\xi_{\{e\}}, [\mathbf{x}'_{\{e\}}, \mathbf{z}_{\{e\}}], \mathbf{y}) = 0 \\ \mathbf{z}_{\{1\}} = \mathbf{z}_{\{2\}} = \dots = \mathbf{z}_{\{Nums(\mathcal{E})\}} \end{cases} \end{aligned}$$

$$\forall e \in \mathcal{E}, \quad (40a)$$

where  $\mathbf{z}_{\{e\}}$  denotes the boundary variables in extreme scenario#  $e$ . This compulsory constraint can be fulfilled as long as we put  $\mathbf{z}_{\{e\}}$  into the first-stage decision-making. Consequently, (40a) has an equivalent formulation, such that:

$$\begin{aligned} & \min \sum_e f(\boldsymbol{\xi}_{\{e\}}, [\mathbf{x}'_{\{e\}}, \mathbf{z}], \mathbf{y}) \\ & \text{s.t.} \begin{cases} \mathcal{G}'_1(\boldsymbol{\xi}_{\{e\}}, \mathbf{x}'_{\{e\}}, \mathbf{y}') \leq 0 \\ \mathcal{H}'(\boldsymbol{\xi}_{\{e\}}, \mathbf{x}'_{\{e\}}, \mathbf{y}') = 0 \\ \mathcal{G}'_2(\mathbf{x}'_{\{e\}}) \leq 0 \end{cases} \\ & \forall e \in \mathcal{E}, \end{aligned} \quad (40b)$$

$$\begin{cases} \mathcal{G}'_{1,\{e\}} := \mathbf{A}_G \boldsymbol{\xi}_{\{e\}}^\top + \mathbf{B}'_G \mathbf{x}'_{\{e\}}^\top + \mathbf{C}'_G \mathbf{y}'^\top \\ \quad = \mathbf{A}_G \boldsymbol{\xi}_{\{e\}}^\top + \mathbf{B}'_G \mathbf{x}'_{\{e\}}^\top + \mathbf{D}_G \mathbf{z}^\top + \mathbf{C}'_G \mathbf{y}'^\top \leq 0 \\ \mathcal{H}'_{\{e\}} := \mathbf{A}_H \boldsymbol{\xi}_{\{e\}}^\top + \mathbf{B}'_H \mathbf{x}'_{\{e\}}^\top + \mathbf{C}'_H \mathbf{y}'^\top \\ \quad = \mathbf{A}_H \boldsymbol{\xi}_{\{e\}}^\top + \mathbf{B}'_H \mathbf{x}'_{\{e\}}^\top + \mathbf{D}_H \mathbf{z}^\top + \mathbf{C}'_H \mathbf{y}'^\top = 0 \\ \mathcal{G}'_{2,\{e\}} := \|\mathbf{E}' \circ \mathbf{x}'_{\{e\}}\|_2 - \mathbf{F}' \mathbf{x}'_{\{e\}}^\top \leq 0 \end{cases}, \quad (40c)$$

$$\begin{cases} \mathbf{B}_{G/H} := [\mathbf{B}'_{G/H}, \mathbf{D}_{G/H}] \\ \mathbf{C}'_{G/H} := [\mathbf{D}_{G/H}, \mathbf{C}'_{G/H}] \\ \mathbf{E} := [\mathbf{E}', \mathbf{0}] \\ \mathbf{F} := [\mathbf{F}', \mathbf{0}] \\ \mathbf{x}_{\{e\}} := [\mathbf{x}'_{\{e\}}, \mathbf{z}_{\{e\}}] \\ \mathbf{y}' := [\mathbf{z}, \mathbf{y}] \end{cases}, \quad (40d)$$

where  $\mathcal{G}'_1(\boldsymbol{\xi}_{\{e\}}, \mathbf{x}'_{\{e\}}, \mathbf{y}') := \mathcal{G}'_{1,\{e\}}$ ,  $\mathcal{G}'_2(\mathbf{x}'_{\{e\}}) := \mathcal{G}'_{2,\{e\}}$ ,  $\mathcal{H}(\boldsymbol{\xi}_{\{e\}}, \mathbf{x}'_{\{e\}}, \mathbf{y}') := \mathcal{H}_{\{e\}}$ . It is evident that the feasible region concerning  $\mathbf{x}_{\{e\}}$  in (40a) is contained in the counterpart of (35). It further implies that the condition that  $\mathbf{y}'$  makes  $\mathbf{x}'_{\{e\}}$  has feasible solutions in (40b) is sufficient for the condition that  $\mathbf{y}$  makes  $\mathbf{x}_{\{e\}}$  in (35) has feasible solutions. As formulated in (4), the boundary variables are not involved in SOCP constraint. Therefore, as formulated in (40c), different from  $\mathcal{G}'_{1,\{e\}}$  and  $\mathcal{H}'_{\{e\}}$ ,  $\mathcal{G}'_{2,\{e\}}$  contains  $\mathbf{x}'_{\{e\}}$  without  $\mathbf{z}_{\{e\}}$ . The changes of the coefficients and variables in 40(a) can be found in (40d).

We assume that the constructed OPF problem formulated as (1)–(24) can be decomposed into  $\mathbb{M}$  blocks according to the decomposition approach provided in (25)–(28). In this case, we have that:

$$\begin{cases} \mathbf{A}_{G/H} := [\mathbf{A}_{G/H}^{[1]}, \mathbf{A}_{G/H}^{[2]}, \dots, \mathbf{A}_{G/H}^{[\mathbb{M}]}] \\ \mathbf{B}'_{G/H} := [\mathbf{B}'_{G/H}^{[1]}, \mathbf{B}'_{G/H}^{[2]}, \dots, \mathbf{B}'_{G/H}^{[\mathbb{M}]}] \\ \mathbf{C}_{G/H} := [\mathbf{C}_{G/H}^{[1]}, \mathbf{C}_{G/H}^{[2]}, \dots, \mathbf{C}_{G/H}^{[\mathbb{M}]}] \\ \mathbf{C}'_{G/H} := [\mathbf{C}'_{G/H}^{[1]}, \mathbf{C}'_{G/H}^{[2]}, \dots, \mathbf{C}'_{G/H}^{[\mathbb{M}]}] \\ \mathbf{D}_{G/H} := [\mathbf{D}_{G/H}^{[1]}, \mathbf{D}_{G/H}^{[2]}, \dots, \mathbf{D}_{G/H}^{[\mathbb{M}]}] \\ \mathbf{E}' := [\mathbf{E}'^{[1]}, \mathbf{E}'^{[2]}, \dots, \mathbf{E}'^{[\mathbb{M}]}] \\ \mathbf{H}' := [\mathbf{H}'^{[1]}, \mathbf{H}'^{[2]}, \dots, \mathbf{H}'^{[\mathbb{M}]}] \end{cases}, \quad (41a)$$

$$\begin{cases} \boldsymbol{\xi}_{\{e\}} := [\boldsymbol{\xi}_{\{e\}}^{[1]}, \boldsymbol{\xi}_{\{e\}}^{[2]}, \dots, \boldsymbol{\xi}_{\{e\}}^{[\mathbb{M}]}] \\ \mathbf{x}'_{\{e\}} := [\mathbf{x}'_{\{e\}}^{[1]}, \mathbf{x}'_{\{e\}}^{[2]}, \dots, \mathbf{x}'_{\{e\}}^{[\mathbb{M}]}] \\ \mathbf{z}_{\{e\}} := [\mathbf{z}_{\{e\}}^{[1]}, \mathbf{z}_{\{e\}}^{[2]}, \dots, \mathbf{z}_{\{e\}}^{[\mathbb{M}]}] \\ \mathbf{y} := [\mathbf{y}^{[1]}, \mathbf{y}^{[2]}, \dots, \mathbf{y}^{[\mathbb{M}]}] \\ \mathbf{y}' := [\mathbf{y}'^{[1]}, \mathbf{y}'^{[2]}, \dots, \mathbf{y}'^{[\mathbb{M}]}] \end{cases}, \quad (41b)$$

$$\begin{cases} \mathcal{G}'_{1,\{e\}} := \mathcal{G}'_{1,\{e\}}^{[1]} \cup \mathcal{G}'_{1,\{e\}}^{[2]} \dots \cup \mathcal{G}'_{1,\{e\}}^{[\mathbb{M}]} \\ \mathcal{H}'_{\{e\}} := \mathcal{H}'_{\{e\}}^{[1]} \cup \mathcal{H}'_{\{e\}}^{[2]} \dots \cup \mathcal{H}'_{\{e\}}^{[\mathbb{M}]} \cup \mathbf{G} \mathbf{z}_{\{e\}}^\top = 0 \\ \mathcal{G}'_{2,\{e\}} := \mathcal{G}'_{2,\{e\}}^{[1]} \cup \mathcal{G}'_{2,\{e\}}^{[2]} \dots \cup \mathcal{G}'_{2,\{e\}}^{[\mathbb{M}]} \end{cases}, \quad (41c)$$

$$\begin{cases} \mathcal{E} := (\mathcal{E}^{[1]}, \mathcal{E}^{[2]}, \dots, \mathcal{E}^{[\mathbb{M}]}) \\ e := (e^{[1]}, e^{[2]}, \dots, e^{[\mathbb{M}]}) \\ \forall e^{[1]} \in \mathcal{E}^{[1]} \\ \forall e^{[2]} \in \mathcal{E}^{[2]} \\ \vdots \\ \forall e^{[\mathbb{M}]} \in \mathcal{E}^{[\mathbb{M}]}, \end{cases} \quad (41d)$$

where  $(\cdot)_{\{e\}}^{[n]}$  corresponds to the parameters, variables, constraints, and sets for block#  $n$  in extreme scenario#  $e$ .  $\mathbf{G} \mathbf{z}_{\{e\}}^\top := \mathbf{G}[\mathbf{z}_{\{e\}}^{[n]}, \mathbf{z}_{\{e\}}^{[1]}, \dots, \mathbf{z}_{\{e\}}^{[\mathbb{M}]}]^\top = 0$  represents the boundary coupling constraint, which emerges after system decomposition and can be used to maintain consistency regarding boundary variables. Particularly, (41d) implies that extreme scenario#  $e$  associated with the complete system can be regarded as a combination of extreme#  $e^{[n]}$  associated with the decomposed system. For the sake of clarity, we call the former as “global” extreme scenario and the latter as the “local” extreme scenario, which yields the following:

$$\text{Nums}(\mathcal{E}) = \prod_{n=1}^{\mathbb{M}} \text{Nums}(\mathcal{E}^{[n]}). \quad (42)$$

For (35), the corresponding distributed OPF problem for block#  $n$  is expressed as below:

$$\begin{aligned} & \min \sum_e f(\boldsymbol{\xi}_{\{e\}}^{[n]}, [\mathbf{x}_{\{e\}}^{[n]}, \mathbf{z}_{\{e\}}^{[n]}], \mathbf{y}^{[n]}) \\ & \text{s.t.} \begin{cases} \mathcal{G}'_{1,\{e\}} := \mathbf{A}_G^{[n]} \boldsymbol{\xi}_{\{e\}}^{[n]\top} + \mathbf{B}'_G^{[n]} \mathbf{x}'_{\{e\}}^{[n]\top} + \mathbf{D}_G^{[n]} \mathbf{z}_{\{e\}}^{[n]\top} \\ \quad + \mathbf{C}_G^{[n]} \mathbf{y}^{[n]\top} \leq 0 \\ \mathcal{H}'_{\{e\}} := \mathbf{A}_H^{[n]} \boldsymbol{\xi}_{\{e\}}^{[n]\top} + \mathbf{B}'_H^{[n]} \mathbf{x}'_{\{e\}}^{[n]\top} + \mathbf{D}_H^{[n]} \mathbf{z}_{\{e\}}^{[n]\top} \\ \quad + \mathbf{C}_H^{[n]} \mathbf{y}^{[n]\top} = 0 \\ \mathcal{G}'_{2,\{e\}} := \|\mathbf{E}'^{[n]} \circ \mathbf{x}'_{\{e\}}^{[n]\top}\|_2 - \mathbf{F}'^{[n]} \mathbf{x}'_{\{e\}}^{[n]\top} \leq 0 \\ \mathbf{G}[\mathbf{z}_{\{e\}}^{[n]}, \widehat{\mathbf{z}}_{\{e\}}^{[1]}, \dots, \widehat{\mathbf{z}}_{\{e\}}^{[\mathbb{M}]}]^\top = 0 \end{cases} \\ & \forall e \in \mathcal{E}. \end{aligned} \quad (43)$$

From (43) we can see that due to the existence of the coupling constraint that  $\mathbf{G}[\mathbf{z}_{\{e\}}^{[n]}, \widehat{\mathbf{z}}_{\{e\}}^{[1]}, \dots, \widehat{\mathbf{z}}_{\{e\}}^{[\mathbb{M}]}]^\top = 0$ , the decision-making of block#  $n$  is not only influenced by “local” extreme scenarios of itself but also “local” extreme scenarios of other

blocks. Consequently, in every specific “local” scenario  $\widehat{e}^{[n]}$ , block#  $n$  still need to consider extreme scenarios associated with other blocks, the number of these extreme scenarios as total as:

$$\begin{cases} Num_s(\mathcal{E}') = \prod_{k=1, k \neq n}^M Num_s(\mathcal{E}^{[k]}) \\ e' := (\widehat{e}^{[n]}, e^{[1]}, \dots, e^{[M]}) \\ e' \in \mathcal{E}'. \end{cases} \quad (44)$$

According to (44), it can be deduced that despite the distributed optimization model built, each block still needs to consider an equal number of “global” extreme scenarios, as mentioned in (35).  $\mathcal{E}'$  denotes the set that covers all extreme scenarios associated with other blocks.

For (40), the corresponding distributed OPF problem for block#  $n$  is expressed as below:

$$\begin{aligned} & \min \sum_e f \left( \xi_{\{e\}}^{[n]}, \left[ \mathbf{x}_{\{e\}}^{[n]}, \mathbf{z}^{[n]} \right], \mathbf{y}^{[n]} \right) \\ & \text{s.t.} \begin{cases} \mathcal{G}_{1,\{e\}}^{[n]} := \mathbf{A}_{\mathcal{G}}^{[n]} \xi_{\{e\}}^{[n]\top} + \mathbf{B}_{\mathcal{G}}^{[n]} \mathbf{x}_{\{e\}}^{[n]\top} + \mathbf{C}_{\mathcal{G}}^{[n]} \mathbf{y}^{[n]\top} \leq 0 \\ \mathcal{H}_{\{e\}}^{[n]} := \mathbf{A}_{\mathcal{H}}^{[n]} \xi_{\{e\}}^{[n]\top} + \mathbf{B}_{\mathcal{H}}^{[n]} \mathbf{x}_{\{e\}}^{[n]\top} + \mathbf{C}_{\mathcal{H}}^{[n]} \mathbf{y}^{[n]\top} = 0 \\ \mathcal{G}_{2,\{e\}}^{[n]} := \|\mathbf{E}'^{[n]} \circ \mathbf{x}_{\{e\}}^{[n]\top}\|_2 - \mathbf{F}'^{[n]} \mathbf{x}_{\{e\}}^{[n]\top} \leq 0 \\ \mathbf{G} \left[ \mathbf{z}^{[n]}, \widehat{\mathbf{z}}^{[1]}, \dots, \widehat{\mathbf{z}}^{[M]} \right]^\top = 0 \end{cases} \\ & \forall e \in \mathcal{E}. \end{aligned} \quad (45a)$$

From (45a), we can observe that  $\mathbf{G} \left[ \mathbf{z}^{[n]}, \widehat{\mathbf{z}}^{[1]}, \dots, \widehat{\mathbf{z}}^{[M]} \right]^\top = 0$  makes the decision-making of block#  $n$  exclusively influenced by “local” extreme scenarios of itself but not “local” extreme scenarios of other blocks. In this case, many constraints linked with “global” extreme scenarios are redundant, and (45a) is equal to a reduced version, such that:

$$\begin{aligned} & \min \sum_{e^{[n]}} f \left( \xi_{\{e^{[n]}\}}^{[n]}, \left[ \mathbf{x}_{\{e^{[n]}\}}^{[n]}, \mathbf{z}^{[n]} \right], \mathbf{y} \right) \\ & \text{s.t.} \begin{cases} \mathcal{G}_{1,\{e^{[n]}\}}^{[n]} := \mathbf{A}_{\mathcal{G}}^{[n]} \xi_{\{e^{[n]}\}}^{[n]\top} + \mathbf{B}_{\mathcal{G}}^{[n]} \mathbf{x}_{\{e^{[n]}\}}^{[n]\top} + \mathbf{C}_{\mathcal{G}}^{[n]} \mathbf{y}^{[n]\top} \leq 0 \\ \mathcal{H}_{\{e^{[n]}\}}^{[n]} := \mathbf{A}_{\mathcal{H}}^{[n]} \xi_{\{e^{[n]}\}}^{[n]\top} + \mathbf{B}_{\mathcal{H}}^{[n]} \mathbf{x}_{\{e^{[n]}\}}^{[n]\top} + \mathbf{C}_{\mathcal{H}}^{[n]} \mathbf{y}^{[n]\top} = 0 \\ \mathcal{G}_{2,\{e^{[n]}\}}^{[n]} := \|\mathbf{E}'^{[n]} \circ \mathbf{x}_{\{e^{[n]}\}}^{[n]\top}\|_2 - \mathbf{F}'^{[n]} \mathbf{x}_{\{e^{[n]}\}}^{[n]\top} \leq 0 \\ \mathbf{G} \left[ \mathbf{z}^{[n]}, \widehat{\mathbf{z}}^{[1]}, \dots, \widehat{\mathbf{z}}^{[M]} \right]^\top = 0 \end{cases} \\ & \forall e^{[n]} \in \mathcal{E}^{[n]}. \end{aligned} \quad (45b)$$

Equation (45b) indicates that when the distributed optimization approach is taken, each block only needs to consider their own “local” extreme scenarios instead of “global” extreme scenarios.

In summary, (45) offers a distributed optimization approach for (40), significantly reducing the number of extreme scenarios that need to be considered. Equation (40) provides a more conservative optimization result than (35) due to the added compulsory constraint associated with boundary variables. Besides, it also means that if (40) has feasible solutions, then (35) definitely

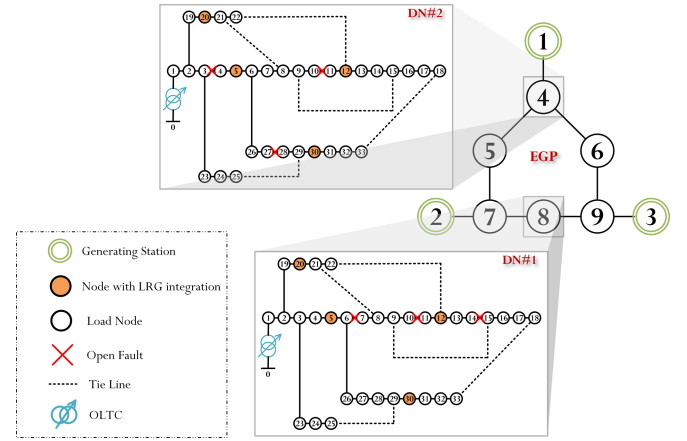


Fig. 8. Configuration of an integrated test system of one EPG and two DNs.

has feasible solutions. Further, once (35) has feasible solutions, the initial problem (34) will also have feasible solutions. Eventually, we can conclude that the distributed optimization model (45b) can provide a robust decision-making regarding DN reconfiguration to hedge the uncertainties origin from LRG, by considering the reduced number of extreme scenarios.

## V. CASE STUDY

As presented in Fig. 8, the integrated test system consists of one IEEE 9-bus EPG and two modified IEEE 33-bus DNs. In both DN#1 and DN#2, LRG is integrated into bus#5, bus#12, bus#20, and bus#30, with a rated capacity of 600kW. The uncertain interval of MPPT power for each LRG is [240, 480] kW. In DN#1, line#6-#7, line#10-#11, and line#14-#15 suffer open fault. In DN2, line#3-#4, line#10-#11, and line#27-#28 suffer open fault. In EPG, the rated capacity of generating system at bus#1, bus#2, and bus#3 are 150MVA, 200MVA, and 150MVA, respectively. Their power factor limits are  $\pm 0.85$ . OLTC has 17 tap positions with a voltage regulating range of  $\pm 1.25\% \times 8$ . The voltage safety bound for EPG and DNs are [0.97, 1.1] p.u. and [0.95, 1.05] p.u., respectively. The voltage bound regarding the LDC dead-band zone for LRG is [0.98, 1.02] p.u.

In particular, for asynchronous implementation in distributed optimization, we assume that EPG and DN#2 spend the same amount of time on computation and communication, while DN#1 spends twice as much time on the counterpart. It means that the variables between EPG and DN#2 are updated every iteration, while between EPG and DN#1 are updated every two iterations. Thanks to the application of the extreme scenario method in the proposed distributed OPF model, each DN only needs to consider own  $2^4$  “local” extreme scenarios rather than entire  $2^8$  “global” extreme scenario.

The optimization computation is coded on MATLAB with the collaboration of YALIMP. GUROBI is utilized to solve the involved SOCP and MIQP problems on EPG and DN sides, respectively. During each iteration of ATC, ADMM, and APP, the corresponding OPF problems related to DN#1 and DN#2 are processed simultaneously, invoking “parfor” command.

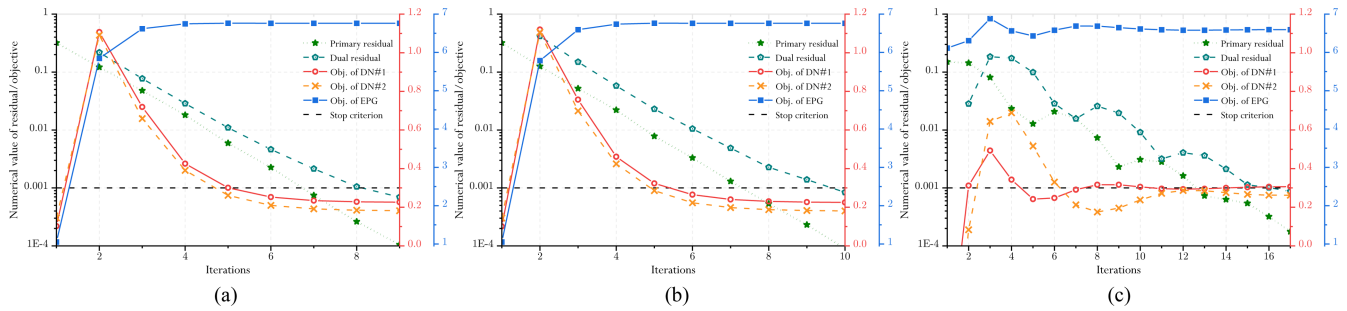


Fig. 9. Convergence performances. (a) Is the distributed optimization result of taking ATC. (b) Is the distributed optimization result of taking ADMM. (c) Is the distributed optimization result of taking APP.

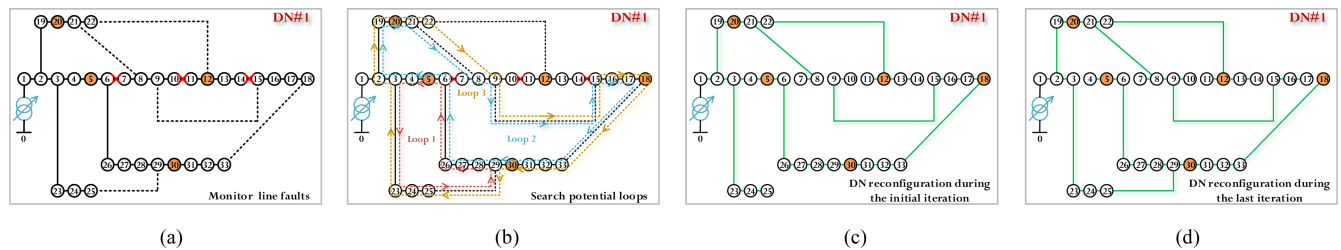


Fig. 10. Reconfiguration procedure of DN #1 (taking ADMM). (a) Shows DN with the line open fault before reconfiguration. (b) Shows potential loops in DN. (c) Shows DN reconfiguration in the initial iteration. (d) Shows DN reconfiguration in the last iteration.

“allcycles” command is used to help search potential loops during the process of DN reconfiguration.

#### A. Convergence Discussion Regarding Distributed Optimization Method

Distributed optimization among DN and EGP is accomplished through information exchanges on the boundary node. The stop criterion related to the boundary residuals is  $1e-3$ , which is relatively loose for avoiding iteration entering the endless loop.

Fig. 9 presents the convergence performances of taking standard ATC, ADMM, and APP, respectively: Although the constructed OPF model with integer variables is not a typical convex problem, all of the distributed optimization methods adopted still have fulfilled the stop criterion after several iterations. Moreover, because ATC and ADMM have highly similar iteration expressions, the optimization objectives of DN#1, DN#2, and EPG mostly converge to the same numerical values. Besides, the reconfigured topology of DN eventually converged to a determined shape after several iterations.

Fig. 10 illustrates the reconfiguration procedure of DN#1 with taking ADMM: After monitoring line open faults in Fig. 10(a), a total of three potential loops are identified and marked in Fig. 10(b). Fig. 10(c) and (d) present the reconfigured network topologies during the initial and last iteration, respectively. It is evident that the two topologies are different. As a result, we can conclude that considering EGP impacts on DN root voltage is vital for effective DN reconfiguration. Neglecting the influence of EGP operation on the DN root node voltage can significantly affect the decision-making process regarding the reconfigured topology.

TABLE I  
DISTRIBUTED OPTIMIZATION PERFORMANCES WITH DIFFERENT APPROACHES

Methods	Approach I		Approach II		Approach III	
	Obj.	Iter.	Obj.	Iter.	Obj.	Iter.
ATC	7.1704	9	7.1790	16	7.1818	17
ADMM	7.1680	10	7.1782	18	7.1782	18
APP	7.1633	17	7.4813	17	7.4865	18

#### B. Comparative Analysis Regarding Distributed Optimization Results

We compare distributed optimization results taking ATC, ADMM, and APP with different implementation approaches. We designate the results achieved through standard processing as **Approach I**, the results obtained through parallel processing as **Approach II**, and the results obtained by considering both parallel processing and asynchronous implementation as **Approach III**. To assess the optimality of the distributed optimization outcomes, we utilize the global optimal numerical result 7.1273 attained through centralized optimization as the benchmark.

Table I presents the optimization performance in terms of optimization objective (the sum of optimized numerical values of optimization objectives in EGP, DN#1 and DN#2) and iteration: A comparison between **Approach I** and **Approach II** reveals that for ATC and ADMM, **Approach II** enables parallel computation but requires more iterations. Although the computation time for each iteration in parallel distributed optimization is shorter, the increased number of iterations makes it challenging to judge which approach has a lower total computation time in practical applications. Regarding APP, the iterations with **Approach I** and **Approach II** are nearly the same. This similarity arises because the standard iteration approach for APP is inherently parallel.

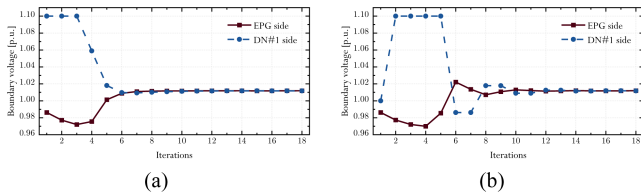


Fig. 11. Iteration curve regarding boundary voltage between EPG and DN #1 side (taking ADMM). (a) Is with Approach II. (b) Is with Approach III.

TABLE II  
COMPARISON OF OPTIMIZATION RESULTS BETWEEN THE DETERMINISTIC APPROACH AND THE PROPOSED ROBUST APPROACH IN DN #1

Approaches	Optimization objective (under 100 random scenarios)			
	Max.	Min.	Avg.	Std.
Deterministic	0.0293	0.0082	0.0096	0.0024
Robust	0.0144	0.0137	0.0140	2.08e-4

Furthermore, regardless of the distributed optimization methods used, **Approach I** yields optimization results that are closer to the global optimal value. This implies that the augmented Lagrangian relaxation method can still guarantee optimality to some extent when applied to the constructed distributed OPF problem that incorporates mixed-integer variables. Comparing **Approach II** and **Approach III**, we observe that even though only partial information regarding boundary variables is available at each iteration, it has a slight impact on optimality and iterations while effectively saving time for one iteration.

Fig. 11 illustrates the boundary voltage between EPG and DN#1 obtained taking ADMM, providing a more intuitive representation of the iteration process with **Approach II** and **Approach III**: By comparing Fig. 11(a) and (b), it is evident that the boundary voltage exhibits more dramatic changes before reaching the final convergence with **Approach III**. This behavior can be attributed to the fact that DN#1 is unable to provide the latest boundary variables to the EPG side in every iteration, leading to more significant variations in the boundary voltage.

### C. Robustness Verification Regarding the Proposed DN Reconfiguration Approach

Traditionally, DN reconfiguration was conducted using the deterministic approach. We randomly generate 100 scenarios regarding LRG to compare the optimization results between the proposed robust approach based on the extreme scenario method and the deterministic approach. For the deterministic approach, the line switch status and OLTC tap position are kept constant for 100 scenarios, which are determined by considering only one expected scenario. For the proposed robust approach, besides the line switch status and OLTC tap position, the boundary voltage and power are also kept constant for 100 scenarios, which are served as the first-stage variables and determined by considering  $2^4$  “local” extreme scenarios.

The comparative results in DN#1 are shown in Table II: We can see that the proposed robust approach has a larger average value for the optimization objective, but it provides stable optimization results encountering the different scenarios and can

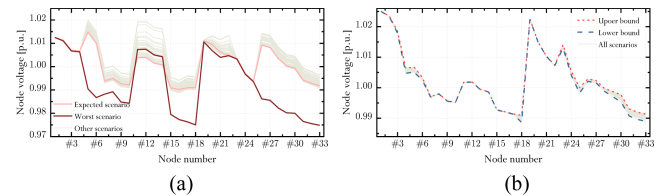


Fig. 12. System-wide voltage profile in DN #1. (a) Is with the deterministic approach. (b) Is with the proposed robust approach.

TABLE III  
ACTIVE POWER LOSSES BEFORE AND AFTER DN RECONFIGURATION

DN	Active power loss (MW)		
	Before reconfig.	After reconfig. (without LDC)	After reconfig. (with LDC)
#1	0.1911	0.0965	0.0553
#2	0.1913	0.0880	0.0711

hedge against any possible realization within the uncertainty related to LRG.

Fig. 12 presents a comparison of the system-wide voltage profiles in DN#1: The expected voltage profile optimized using the deterministic approach appears ideal in Fig. 12(a). However, this optimized profile is highly susceptible to significant deviations in the event of the worst scenario. In contrast, in Fig. 12(b), the proposed strategy demonstrates consistently satisfactory voltage profiles across all scenarios and establishes tight bounds on the voltage profiles. This highlights the robustness of the proposed approach, as it is able to maintain desirable voltage profiles even in different uncertain scenarios.

### D. DN Operation Status After Reconfiguration

The following results from the proposed distributed optimization approach are obtained to better demonstrate the effectiveness of the proposed DN reconfiguration approach (we select the results based on ADMM to present).

Firstly, we compare the power flow before and after reconfiguration in Fig. 13 (here line open faults are not considered for DN before reconfiguration): Quite a few branches have heavy power flow before reconfiguration in Fig. 13(a). Thanks to the reconfigured DN topology as well as the power generation of LRG, the system-wide branch power flows in Fig. 13(b) and (c) are slighter than those before reconfiguration.

Fig. 14 depicts the system-wide voltage profiles before and after DN reconfiguration: Thanks to the appropriate reconfigured DN topology and sufficient power support from LRG, the node voltages across the entire system have been optimized to ensure that they fall within the voltage safety bounds. Notably, as shown in Fig. 14(b), even with LRG integration but no LDC, the node voltage profile in DN#2 still fails to fall in the allowable voltage bound, i.e., [0.95, 1.05] p.u.

Moreover, as shown in Table III: The optimization of active power loss is also achieved effectively. With the local load supply by LRG and the optimized reconfigured DN topology, the burden of power flow on branches is alleviated, resulting in a reduction in active power losses. Additionally, LRG plays a further role in optimizing power losses by using LDC.

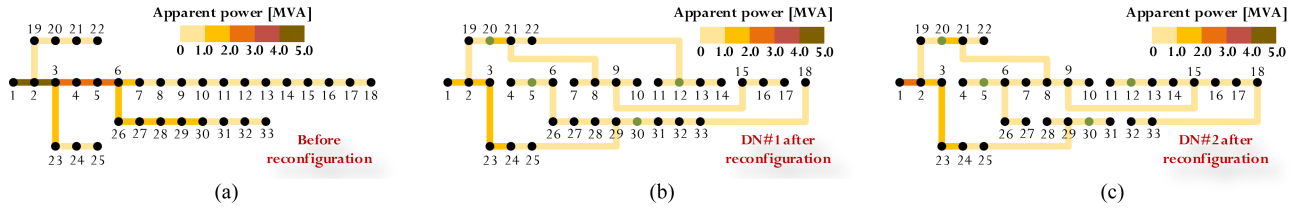


Fig. 13. Power flow profiles before and after reconfiguration. (a) Is the original power flow profile before reconfiguration. (b) Is the power flow profile after reconfiguration for DN #1. (c) Is the power flow profile after reconfiguration for DN #2. Green nodes refers to the integration location of LRG.

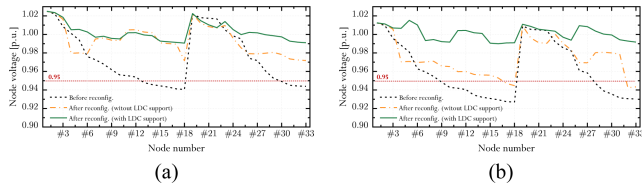


Fig. 14. System-wide voltage profiles before and after reconfiguration. (a) Shows the voltage profiles in DN #1. (b) Shows the voltage profiles in DN #2.

## VI. CONCLUSION

We have demonstrated an optimal DN reconfiguration approach, considering the impacts of EPG and LRG on DN. To address this issue that EPG operation affects DN root voltage, we have developed a mixed-integer convex OPF model that incorporates EPG and DN sides and embeds the LDC function. The distributed optimization methods based on the augmented Lagrangian relaxation have been employed to solve the constructed OPF model. To address this challenge that the integration of LRG introduces uncertainty in the system-wide power flow within the DN, we have introduced the extreme scenario method to generate robust decision-making. Based on our comprehensive numerical results, we draw the following main conclusions:

- 1) Despite the inclusion of mixed-integer variables in the proposed OPF model, ATC, ADMM, and APP still exhibit satisfactory performance in terms of optimality and convergence for distributed optimization. The parallel approach effectively reduces computation time for each iteration through parallel processing. However, it also leads to an increase in the overall number of iterations. As for the asynchronous implementation, it makes the convergence process concerning boundary variables fluctuate more significantly, but it is still an appropriate way to save computation time in one iteration and it affects the final convergent result slightly.
- 2) The introduction of the extreme scenario method enables the proposed DN reconfiguration to provide a robust decision-making when confronted with uncertain scenarios associated with LRG integration. Furthermore, applying the extreme scenario method in distributed optimization considerably reduces the number of extreme scenarios that need to be taken into account, thereby alleviating the computational burden.
- 3) Thanks to the DN reconfiguration and LRG power support, the heavy power flow on certain branches is mitigated in

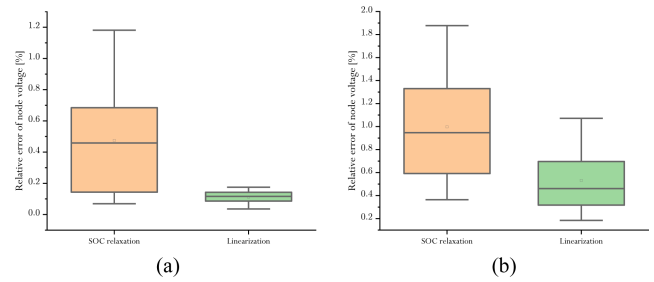


Fig. 15. Statistical distribution regarding relative error for node voltage. (a) Is based on PG&E 69-bus system. (b) Is based on IEEE 85-bus system.

DN. More importantly, the system-wide voltage profile is improved and the active power loss is reduced for DN.

## APPENDIX

### A. Selection of Power Flow Constraint in DN

Linearization and SOC relaxation are two commonly used approaches to handle the DistFlow model, forming the power flow constraint in DN. Linearized DistFlow has been presented in (5). SOC relaxation of DistFlow is shown as follows:

$$\begin{cases} p_i = \sum_j p_{ij} - p_{hi} + r_{ij} l_{ij} \\ q_i = \sum_j q_{ij} - q_{hi} + x_{ij} l_{ij} \\ u_i - u_j = 2(r_{ij} p_{ij} + x_{ij} q_{ij}) - (r_{ij}^2 + x_{ij}^2) l_{ij} \\ p_{ij}^2 + q_{ij}^2 \leq u_i l_{ij} \end{cases}, \quad \forall i, j \in \mathcal{N}_{\text{DN}}, \forall ij, h_i \in \mathcal{l}_{\text{DN}}, \forall h \in \mathcal{F}_i, \forall j \in \mathcal{D}_i, \quad (46)$$

where  $l_{ij}$  represents the square of branch current. The corresponding optimization objective is formulated as:

$$\begin{aligned} \min f_{\text{DN}} := & \sum_{ij} r_{ij} l_{ij} + \sum_i (u_i - 1)^2 \\ & ij \in \mathcal{l}_{\text{DN}}, i \in \mathcal{N}_{\text{DN}}. \end{aligned} \quad (47)$$

We utilize PG&E 69-bus and IEEE 85-bus systems as the case system, and randomly generate 100 scenarios linked with active loads data to support OPF computation (node reactive power injection is regarded as the optimization variable). Then, we make statistics on the relative error between the approximate value of node voltage that is computed via the constructed OPF model and the actual value of node voltage that is computed via the Newton-Raphson method.

It can be seen from Fig. 15: The relative error of node voltage with SOC relaxation on DistFlow is much larger than the counterpart with linearization on DistFlow. It indicates that

linearization on DistFlow outperforms SOC relaxation on DistFlow in terms of solving the proposed OPF problem with the optimization objective that contains both minimizing the node voltage deviation and the active power loss.

### B. Modified Optimal DN Reconfiguration Model for LDC With $q(v)$ Type

The approach of embedding the LDC with  $q(v)$  into the constructed OPF model to take the place of the LDC  $q(u)$  is simple. Only a minor modification is needed that replaces  $\{u_i, u_{i,DB}^{\min}, u_{i,DB}^{\max}, u_i^{\min}, u_i^{\max}\}$  with  $\{v_i, v_{i,DB}^{\min}, v_{i,DB}^{\max}, v_i^{\min}, v_i^{\max}\}$  involved in (19)–(23). However, after that, a challenging problem occurs that  $q(v)$  is with respect to  $v$ , whereas the power flow constraint is with respect to  $u$ . In this case, the nonlinear relationship that  $u_i = v_i^2$  should be appropriately handled and be integrated into (2)–(24) to form a modified OPF model. Next, three widely used approximation approaches are provided to reformulate the quadratic quality constraint  $u_i = v_i^2$ .

*Taylor Expansion:*  $u_i = v_i^2$  can be linearized to a linear constraint, such that (First-order Taylor expansion around 1p.u.):

$$u_i = 1 + 2(v_i - 1), \forall i \in \mathcal{N}_{DN}. \quad (48)$$

*McCormick Relaxation:* McCormick relaxation handles  $u_i = v_i^2$  by adding a series of auxiliary constraints. Particularly, the piecewise McCormick relaxation [49] is able to provide a tighter convex envelop via multiple partitioning. We present  $u_i = v_i^2$  relaxed by a bivariate piecewise form as below (the bound  $v_i \in [0.95, 1.05]$ p.u. is divided into five partitions):

$$\begin{cases} u_i \geq \sum_n (2v_{i,n}^{\min} v_{i,n} - v_{i,n}^{\min} v_{i,n}^{\min} \gamma_{i,n}) \\ u_i \geq \sum_n (2v_{i,n}^{\max} v_{i,n} - v_{i,n}^{\max} v_{i,n}^{\max} \gamma_{i,n}) \\ u_i \leq \sum_n (v_{i,n}^{\min} v_{i,n} + v_{i,n}^{\max} v_{i,n} - v_{i,n}^{\min} v_{i,n}^{\max} \gamma_{i,n}) \end{cases}, \quad (49a)$$

$$\begin{cases} u_{i,n}^{\min} \in \{0.95, 0.97, 0.99, 1.01, 1.03\} \text{p.u.} \\ u_{i,n}^{\max} \in \{0.97, 0.99, 1.01, 1.03, 1.05\} \text{p.u.} \end{cases}, \quad (49b)$$

$$\begin{cases} \sum_n \gamma_{i,n} = 1, \gamma_{i,n} \in \{0, 1\} \\ v_{i,n}^{\min} \gamma_{i,n} \leq v_{i,n} \leq v_{i,n}^{\max} \gamma_{i,n} \\ v_i = \sum_n v_{i,n} \end{cases}, \quad (49c)$$

$$\forall n \in \{1, 2, 3, 4, 5\}, \forall i \in \mathcal{N}_{DN}. \quad (49c)$$

*Convex Quadratic Relaxation:* [50] provides a convex quadratic relaxation to  $u_i = v_i^2$ , which can also be further expanded to a bivariate piecewise form, such that:

$$\begin{cases} u_i \geq \sum_n v_{i,n}^2 \\ u_i \leq \sum_n (v_{i,n}^{\min} v_{i,n} + v_{i,n}^{\max} v_{i,n} - v_{i,n}^{\min} v_{i,n}^{\max} \gamma_{i,n}) \end{cases}, \quad (49b) \text{ and } (49c),$$

$$\forall n \in \{1, 2, 3, 4, 5\}, \forall i \in \mathcal{N}_{DN}. \quad (50)$$

We use DN#2 in Fig. 8 as the test system to compare the performances of the above approaches applied in the modified

OPF in terms of  $\|u_i - v_i^2\|_2$ . We would like to emphasize that our focus here is to develop a modified optimal DN reconfiguration model for incorporating the LDC with  $q(v)$  type. Hence, the

TABLE IV  
 $\|u_i - v_i^2\|_2$  FOR EACH APPROXIMATION APPROACH

Taylor expansion	McCormick relaxation	Convex quadratic relaxation
5.6050e-3	2.9429e-4	2.7629e-4

✧ The root voltage is fixed as 0.97p.u. and the deterministic scenario is with  $p_{i,LRG}^{\text{MPPT}} := 320 \text{ kW}$ .

application of the extreme scenario method and the augmented Lagrangian relaxation-based distributed optimization methods are not discussed.

As presented in Table IV: McCormick relaxation and the convex quadratic relaxation excels Taylor expansion. However, Taylor expansion can still become a competitive option since integer variables are not involved to approximate  $u_i = v_i^2$ .

### REFERENCES

- [1] S. Civanlar, J. J. Grainger, H. Yin, and S. S. H. Lee, "Distribution feeder reconfiguration for loss reduction," *IEEE Trans. Power Del.*, vol. 3, no. 3, pp. 1217–1223, Jul. 1988.
- [2] D. Shirmohammadi and H. W. Hong, "Reconfiguration of electric distribution networks for resistive line losses reduction," *IEEE Trans. Power Syst.*, vol. 4, no. 1, pp. 1492–1498, Apr. 1989.
- [3] H. Kim, Y. Ko, and K.-H. Jung, "Artificial neural-network based feeder reconfiguration for loss reduction in distribution systems," *IEEE Trans. Power Del.*, vol. 8, no. 3, pp. 1356–1366, Jul. 1993.
- [4] R. J. Sarfifi, M. M. A. Salama, and A. Y. Chikhani, "Distribution system reconfiguration for loss reduction: An algorithm based on network partitioning theory," *IEEE Trans. Power Syst.*, vol. 11, no. 1, pp. 504–510, Feb. 1996.
- [5] H. Chang and C. Kuo, "Network reconfiguration in distribution systems using simulated annealing," *Electric Power Syst. Res.*, vol. 29, pp. 227–238, 1994.
- [6] R. Pegado, Z. Naupari, Y. Molina, and C. Castillo, "Radial distribution network reconfiguration for power losses reduction based on improved selective BPSO," *Electric Power Syst. Res.*, vol. 169, pp. 206–213, 2019.
- [7] A. Abdelaziz, F. Mohammed, S. Mekhamer, and M. Badr, "Distribution systems reconfiguration using a modified particle swarm optimization algorithm," *Electric Power Syst. Res.*, vol. 79, no. 11, pp. 1521–1530, 2009.
- [8] C. Wang and Y. Gao, "Determination of power distribution network configuration using non-revisiting genetic algorithm," *IEEE Trans. Power Syst.*, vol. 28, no. 4, pp. 3638–3648, Nov. 2013.
- [9] A. M. Eldurssi and R. M. O'Connell, "A fast nondominated sorting guided genetic algorithm for multi-objective power distribution system reconfiguration problem," *IEEE Trans. Power Syst.*, vol. 30, no. 2, pp. 593–601, Mar. 2015.
- [10] A. Y. Abdelaziz, F. M. Mohamed, S. F. Mekhamer, and M. A. L. Badr, "Distribution system reconfiguration using a modified Tabu Search algorithm," *Electric Power Syst. Res.*, vol. 80, pp. 943–953, 2010.
- [11] R. A. Jabr, R. Singh, and B. C. Pal, "Minimum loss network reconfiguration using mixed-integer convex programming," *IEEE Trans. Power Syst.*, vol. 27, no. 2, pp. 1106–1116, May 2012.
- [12] L. Qiao, Y. Tan, and D. Kirschen, "An ILP algorithm for feeder reconfiguration under capacity constraints," in *Proc. IEEE Power Energy Soc. Gen. Meeting*, 2020, pp. 1–5.
- [13] M. E. Baran and F. F. Wu, "Network reconfiguration in distribution systems for loss reduction and load balancing," *IEEE Trans. Power Del.*, vol. 4, no. 2, pp. 1401–1407, Apr. 1989.
- [14] J. A. Taylor and F. S. Hover, "Convex models of distribution system reconfiguration," *IEEE Trans. Power Syst.*, vol. 27, no. 3, pp. 1407–1413, Aug. 2012.
- [15] A. Kavousi-Fard and T. Niknam, "Optimal distribution feeder reconfiguration for reliability improvement considering uncertainty," *IEEE Trans. Power Del.*, vol. 29, no. 3, pp. 496–507, Jun. 2014.
- [16] Y. Song, Y. Zheng, T. Liu, S. Lei, and D. J. Hill, "A new formulation of distribution network reconfiguration for reducing the voltage volatility induced by distributed generation," *IEEE Trans. Power Syst.*, vol. 35, no. 1, pp. 496–507, Jan. 2020.

- [17] W. S. Cheng and H. F. Zhang, "A dynamic economic dispatch model in incorporating wind power based on chance constrained programming," *Energies*, vol. 8, no. 1, pp. 233–256, 2015.
- [18] V. Kekatos, G. Wang, A. J. Conejo, and G. B. Giannakis, "Stochastic reactive power management in microgrids with renewables," *IEEE Trans. Power Syst.*, vol. 30, no. 6, pp. 3386–3395, Nov. 2015.
- [19] H. Gao, J. Liu, and L. Wang, "Robust coordinated optimization of active and reactive power in active distribution systems," *IEEE Trans. Smart Grid*, vol. 9, no. 5, pp. 4436–4447, Sep. 2018.
- [20] C. Zhang, Y. Xu, Z. Dong, and J. Ravishanker, "Three-stage robust inverter-based voltage/VAR control for distribution networks with high level PV," *IEEE Trans. Smart Grid*, vol. 10, no. 1, pp. 782–793, Jan. 2019.
- [21] J. W. Simpson-Porco, F. Dorfler, and F. Bullo, "Voltage stabilization in microgrids via quadratic droop control," in *Proc. IEEE 52nd Conf. Decis. Control*, 2013, pp. 7582–7589.
- [22] A. Singhal, V. Ajjarapu, J. Fuller, and J. Hansen, "Real-time local volt/var control under external disturbances with high PV penetration," *IEEE Trans. Smart Grid*, vol. 10, no. 4, pp. 3849–3859, Jul. 2019.
- [23] P. Jahangiri and D. C. Aliprantis, "Distributed Volt/VAR Control by PV Inverters," *IEEE Trans. Power Syst.*, vol. 28, no. 3, no. pp. 3429–3439, Aug. 2013.
- [24] Z. Li, Q. Guo, H. Sun, and J. Wang, "Coordinated economic dispatch of coupled transmission and distribution systems using heterogeneous decomposition," *IEEE Trans. Power Syst.*, vol. 31, no. 6, pp. 4817–4830, Nov. 2016.
- [25] Z. Li, Q. Guo, H. Sun, and J. Wang, "Coordinated transmission and distribution AC optimal power flow," *IEEE Trans. Power Syst.*, vol. 9, no. 2, pp. 1228–1240, Mar. 2018.
- [26] H. Li, S. Li, D. Jiang, Q. Guo, and L. Zhou, "Reconfiguration strategy for distribution network considering the impact of external power grid," in *Proc. IEEE 2nd China Int. Youth Conf. Elect. Eng.*, 2021, pp. 1–6.
- [27] H. M. Kim, N. F. Michelena, P. Y. Papalambros, and T. Jiang, "Target cascading in optimal system design," *J. Mech. Des.*, vol. 125, no. 3, pp. 474–480, 2003.
- [28] S. Huang, Q. Wu, J. Zhao, and W. Liao, "Distributed optimal voltage control for VSC-HVDC connected large-scale wind farm cluster based on analytical target cascading method," *IEEE Trans. Sustain. Energy*, vol. 11, no. 4, pp. 2152–2161, Oct. 2020.
- [29] T. Erseghe, "Distributed optimal power flow using ADMM," *IEEE Trans. Power Syst.*, vol. 29, no. 5, pp. 2370–2380, Sep. 2014.
- [30] S. Huang, Q. Wu, Y. Guo, X. Chen, B. Zhou, and C. Li, "Distributed voltage control based on ADMM for large-scale wind farm cluster connected to VSC-HVDC," *IEEE Trans. Sustain. Energy*, vol. 11, no. 2, pp. 584–594, Apr. 2020.
- [31] Q. Zhang, K. Dehghanpour, and Z. Wang, "Distributed CVR unbalanced distribution systems with PV penetration," *IEEE Trans. Smart Grid*, vol. 10, no. 5, pp. 5308–5319, Sep. 2019.
- [32] R. Baldick, B. H. Kim, C. Chase, and Y. Luo, "A fast distributed implementation of optimal power flow," *IEEE Trans. Power Syst.*, vol. 14, no. 3, pp. 858–864, Aug. 1999.
- [33] S. Zhan, J. Morren, W. van Den Akker, A. van der Molen, N. G. Paterakis, and J. G. Slootweg, "Combined MV-LV power grid operation: Comparing sequential, integrated, and decentralized control architectures," in *Proc. Int. Conf. Smart Energy Syst. Technol.*, 2022, pp. 1–6.
- [34] Y. Zhang, X. Ai, J. Fang, W. Yao, and J. Wen, "Two-stage reactive power optimization for distribution network with distributed generation based on extreme scenarios," *Trans. China Electrotech. Soc.*, vol. 33, no. 2, pp. 380–389, 2018.
- [35] J. Xu et al., "A day-ahead economic dispatch method considering extreme scenarios based on wind power uncertainty," *Comput. Sci. Elect. Eng. J. Power Energy Syst.*, vol. 5, no. 2, pp. 224–233, 2019.
- [36] S. Li, L. Wang, X. Gu, H. Zhao, and Y. Sun, "Optimization of loop-network reconfiguration strategies to eliminate transmission line overloads in power system restoration process with wind power integration," *Int. J. Electric Power Energy Syst.*, vol. 134, pp. 1–12, 2022.
- [37] P. N. Yasasvi, S. Chandra, A. Mohapatra, and S. C. Srivastava, "An exact SOCP formulation for AC optimal power flow," in *Proc. 20th Nat. Power Syst. Conf.*, 2018, pp. 1–6.
- [38] M. Farivar, C. R. Clarke, S. H. Low, and M. Chandy, "Inverter VAR control for distribution systems with renewables," in *Proc. IEEE Int. Conf. Smart Grid Commun.*, 2011, pp. 457–462.
- [39] J. A. Taylor, *Convex Optimization of Power Systems*, 1st ed. Cambridge, U.K.: Cambridge Univ. Press, 2015.
- [40] E. Zunic, A. Djedovic, and B. Zunic, "Software solution for optimal planning of sales persons work based on depth-first search and breadth-first search algorithms," in *Proc. 39th Int. Conv. Inf. Commun. Technol., Electron. Microelectronics*, 2016, pp. 1248–1253.
- [41] Y. Wang, P. Liao, J. Zhang, and Q. Lu, "Optimal dispatch method of Park-level integrated energy internet based on average-consensus ADMM distributed algorithm," in *Proc. 40th Chin. Control Conf.*, 2021, pp. 6834–6839.
- [42] T.-H. Chang, M. Hong, W.-C. Liao, and X. Wang, "Asynchronous distributed ADMM for large-scale optimization-part I: Algorithm and convergence analysis," *IEEE Trans. Signal Processing*, vol. 64, no. 12, pp. 3118–3129, Jun. 2016.
- [43] Q. Zhang, Y. Guo, Z. Wang, and F. Bu, "Distributed optimal conservation voltage reduction in integrated primary-secondary distribution systems," *IEEE Trans. Smart Grid*, vol. 12, no. 5, pp. 3889–3900, Sep. 2021.
- [44] A. K. Kargarian, Y. Fu, S. D. Mohammadi, and M. Rais-Rohani, "Optimal operation of active distribution grids: A system of systems framework," *IEEE Trans. Smart Grid*, vol. 5, no. 3, pp. 1228–1237, May 2014.
- [45] M. Hong, Z.-Q. Luo, and M. Razaviyayn, "Convergence analysis of alternating direction method of multipliers for a family of nonconvex problems," *Soc. Ind. Appl. Math. J. Optim.*, vol. 26, no. 1, pp. 337–364, 2016.
- [46] H. Li, K. Guo, G. Hao, M. Mao, and L. Zhou, "Decentralized communication based two-tier volt-var control strategy for large-scale centralized photovoltaic power plant," *IEEE Trans. Sustain. Energy*, vol. 13, no. 1, pp. 592–606, Jan. 2022.
- [47] F. Hansen and G. K. Pedersen, "Jensen's operator inequality," *Bull. London Math. Soc.*, vol. 35, no. 4, pp. 553–564, 2003.
- [48] S. Boyd and L. Vandenberghe, *Convex Optimization*, 1st ed. Cambridge, U.K.: Cambridge Univ. Press, 2004.
- [49] L. S. de Assis, E. Camponogara, E. Zimberg, B. Ferreira, and I. E. Grossmann, "A piecewise McCormick relaxation-based strategy for scheduling operations in a crude oil terminal," *Comput. Aided Chem. Eng.*, vol. 106, pp. 309–321, 2017.
- [50] H. Hijazi, C. Coffrin, and P. Van Hentenryck, "Convex quadratic relaxations for mixed-integer nonlinear programs in power systems," *Math Prog. Comput.*, vol. 9, no. 3, pp. 321–367, 2017.



**Haixiao Li** received the Ph.D. degree in electrical engineering from the School of Electrical Engineering, Chongqing University, Chongqing, China, in 2021. Since 2021, he has been with Chongqing Energy Internet Engineering Technology Research Center, Chongqing University of Technology, Chongqing, where he was a teacher and researcher. He is currently a Guest Postdoc with Delft University of Technology, Delft, The Netherlands. His research interests include planning and control of renewable energy systems.



**Aleksandra Lekić** (Senior Member, IEEE) received the B.Sc, M.Sc, and Ph.D. degrees in electrical engineering from the School of Electrical Engineering, University of Belgrade, Serbia, in 2012, 2013, and 2017, respectively. Between 2012 and 2018, she was a Teaching Assistant with the School of Electrical Engineering, University of Belgrade, and an Assistant Professor from 2018 to 2019. In 2019, she was a Postdoctoral Researcher with the Department of Electrical Engineering (ESAT), KU Leuven, and with the Institute EnergyVille, Genk, Belgium. Since 2020,

she has been a tenured Assistant Professor with the Faculty of Electrical Engineering, Mathematics and Computer Science, Group Intelligent Electrical Power Grids, TU Delft, Delft, The Netherlands. She also leads a team of researchers specializing in the Control of HVDC/AC power systems. She is an Associate Editor of the *International Journal of Electrical Power & Energy Systems*, Elsevier. She is the Technical Director of the Power System Protection Centre. She represents TU Delft in the General Assembly in the CRESYM organization, committed to open-source software development for the electrical grids.



**Shan Li** received the B.S. degree from Hunan University, Changsha, China, in 1985, the M.S. degree from Xi'an University of Technology, Xi'an, China, in 1992, and the Ph.D. degree from Chongqing University, Chongqing, China, in 2009. Since 2006, he has been a Professor with the Chongqing University of Technology, Chongqing. His research interests include integration of distributed energy systems, control of AC/DC converter, and motor drive.



**Guo Qiang** received the B.S. and M.S. degrees from Southwest University, Chongqing, China, in 2007 and 2010, respectively, and the Ph.D. degree in electrical engineering from Chongqing University, Chongqing, in 2015. He is currently an Associate Professor with the School of Electrical and Electronic Engineering, Chongqing University of Technology, Chongqing. His research interests include three-phase PWM rectifiers, high-frequency power conversion, and dc microgrid.



**Dongrong Jiang** received the B.S. degree from China West Normal University, Nanchong, China, in 1995, and the Ph.D. degree from Southwest Jiaotong University, Chengdu, China, in 2006. From 2007 to 2010, he was a Researcher with Postdoctoral Research Workstations, Fujian Electric Power Company and Zhejiang University, Hangzhou, China. He is currently a Professor with the Chongqing University of Technology, Chongqing, China. His research interests include modeling and planning in the power market.



**Lin Zhou** was born in Sichuan, China, in 1961. He received the B.S., M.S. and Ph.D. degrees from the Department of Electrical Engineering, Chongqing University, Chongqing, China, in 1982, 1988, and 2004, respectively. From 2008 to 2009, he was a Visiting Scholar with Durham University, Durham, U.K., where he was a researcher of microgrid and renewable energy generation. He is currently a Professor with Chongqing University. His research interests include power electronic technology and photovoltaic power generation system.